Characterization of Karst Terrain and Regional Tectonics Using Remotely Sensed Data in Jo Daviess County, Illinois

Samuel V. Panno, Donald E. Luman, and Dennis R. Kolata

Circular 589 2015

ILLINOIS STATE
GEOLOGICAL SURVEY
PRAIRIE RESEARCH INSTITUTE

ILLINOIS STATE GEOLOGICAL SURVEY
Prairie Research Institute
University of Illinois at Urbana-Champaign

Front Cover: *Low-altitude oblique photograph of an alfalfa field exhibiting complex networks of vegetated crop lines taken on July 19, 2012, in eastern Jo Daviess County (photograph by S. Panno).*

Characterization of Karst Terrain and Regional Tectonics Using Remotely Sensed Data in Jo Daviess County, Illinois

Samuel V. Panno, Donald E. Luman, and Dennis R. Kolata

Circular 589 2015

ILLINOIS STATE GEOLOGICAL SURVEY
PRAIRIE RESEARCH INSTITUTE

ILLINOIS

ILLINOIS STATE GEOLOGICAL SURVEY
Prairie Research Institute
University of Illinois at Urbana-Champaign
615 E. Peabody Drive
Champaign, Illinois 61820-6918
http://www.isgs.illinois.edu

Note: Google®, ArcGIS®, Google Earth®, and Shape2Earth® are registered trademarks.

Suggested citation:

Panno, S.V., D.E. Luman, and D.R. Kolata, 2015, Characterization of karst terrain and regional tectonics using remotely sensed data in Jo Daviess County, Illinois: Illinois State Geological Survey, Circular 589, 29 p., 1 map, 1:62,500, digital appendix at http://isgs.illinois.edu/publications/c589/appendix.

Contents

List of Tables

List of Figures

INTRODUCTION

An estimated 25% of the bedrock surface area of Illinois is carbonate rock, 35% of which is concentrated within the state's five known karst regions (Weibel and Panno 1997; Figure 1). Karst is defined as "terrain with distinctive hydrology and landforms arising from a combination of high rock solubility and well developed secondary fracture porosity" (Ford and Williams 1992, p. 1). Characteristic features of karst terrain include sinkholes, caves, large springs, fluted rock outcrops, blind valleys, swallow holes, solution-enlarged crevices, and a well-defined epikarst soil–bedrock interface (White 1988). Epikarst is defined by Williams (2008) as the

> highly weathered carbonate bedrock immediately beneath the surface or beneath the soil (when present) or exposed at the surface. Porosity and permeability are higher near the surface than at depth; consequently after recharge, percolating rainwater is detained near the base of the epikarst, the detention ponding producing an epikarstic aquifer. (p. 1)

Carbonate rock at or near the ground surface is typically fractured on a regional basis because of ancient or modern tectonic stress (Nelson 1995). Movement of surface water and shallow groundwater is initially a diffuse flow through the rock matrix and fractures. Recharge into and through these fractures can enlarge them by dissolution of the calcite and dolomite that constitute the carbonate rock. Eventually, the fractures, including bedding planes, become crevices that result in a greater storage capacity, more rapid recharge, and more rapid movement of groundwater. When the crevices become wide enough (>1 cm or ~0.4 in.; W.B. White, personal communication, 2005), the rock body can possess matrix, fracture, and conduit flow regimes and be classified as a karst aquifer (Quinlan et al. 1991; Ford and Williams 1992).

The study area for this investigation is Jo Daviess County, Illinois, which is situated within the Driftless Area encompassing southwestern Wisconsin, northeastern Iowa, and parts of northwestern Illinois (Figure 1). The bedrock surface consists of Upper Ordovician [443–460 million years ago (Ma)] carbonate rocks of the Galena and Platteville Groups, shale of the Maquoketa Shale, and Silurian-age (412–443 Ma) dolomite that makes up much of the upland areas (see Map 1). Because carbonate bedrock within the Driftless Area karst region in northwestern Illinois is typically overlain by unconsolidated deposits that include loess and residuum (Panno et al. 1997), direct observation of fractures and crevices is limited to the sparse occurrences of road cuts, quarries, and outcrops where bedrock is exposed at the ground surface.

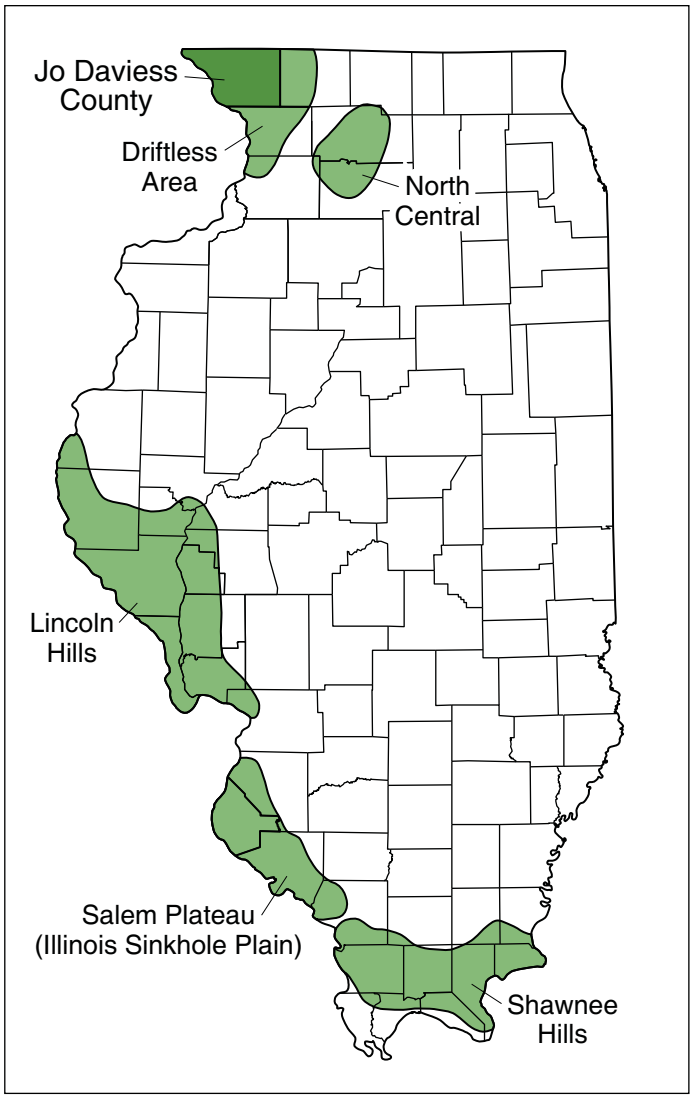

Figure 1 Karst regions of Illinois (Weibel and Panno 1997).

The fractures and crevices of the carbonate bedrock make up the connected secondary porosity of the primary karst aquifer within the study area, which is composed of dolomites of the Galena and Platteville Groups. Most of the rural area, as well as some urbanized areas within the county, depend on this aquifer as an important freshwater resource. Understanding the character of this aquifer and its susceptibility to surface-borne contaminants is necessary to protect and maintain the integrity of this water resource. The lack of sufficient and well-distributed bedrock exposures has made it difficult to develop a comprehensive understanding of the character

Figure 2 Ground photograph of a complex network of vegetated crop lines within an alfalfa field taken on July 19, 2012, in eastern Jo Daviess County (areas ST 4 and CL 9, Map 1 T29N, R5E; see Figures A1–A2 and Tables A1–A2). Normally at this time of year, the alfalfa field would have been cut and harvested for hay. Instead, much of the field exhibits stunted and sparse plant growth (photograph by S. Panno).

and geometry of the fractures and crevices of the karst aquifer within the study area. However, an unforeseen outcome of the severe 2012 summer drought in the Midwest was that it provided a rare opportunity for indirect examination of the fractured and creviced buried bedrock surface of the Driftless Area. Complex vegetated networks, herein referred to as vegetated crop lines, began to appear across the dry summer landscape of Jo Daviess County (Figures 2 and 3), adjacent Stephenson and Carroll Counties in Illinois, and a portion of southwestern Wisconsin. Primarily confined to alfalfa hayfields, the vegetated crop lines resulted from a combination of three factors: (1) persistent, extremely dry conditions; (2) a relatively thin soil zone and associated unconsolidated deposits approximately 1.5 to 6.5 ft (0.5 to 2 m) in thickness overlying (3) highly fractured and creviced bedrock composed of Ordovician-age Galena Dolomite (see Map 1). Corroborating evidence of additional fractures and crevices came from interpretation of enhanced elevation data acquired for Jo Daviess County in 2008 with light detection and ranging (LiDAR) technology.

The primary objectives of this investigation were (1) to analyze remote sensing data resources, including multidate aerial photography collected during the 2012 summer drought depicting vegetated crop lines, and recent LiDAR elevation data to provide new insights regarding the karst aquifer of the Galena Dolomite and karst features within the Silurian dolomite; and (2) to relate the findings to previous research on fractures and crevices to better understand the geology and hydrogeology within the study area. This information will provide a focus for future investigations on the geology as well as on the quality and quantity of groundwater resources in the study area.

REGIONAL GEOLOGIC SETTING OF JO DAVIESS COUNTY

Bedrock within Jo Daviess County is dominated by Ordovician Galena Dolomite, Maquoketa Shale, and Silurian dolomite. The Galena Dolomite and Maquoketa Shale make up the bedrock of the picturesque hills and valleys of the county, whereas the Silurian dolomite is the cap rock responsible for the distinctive bedrock knobs and highlands. Additionally, the Galena Group and underlying Platteville Group constitute an important and reliable groundwater resource, collectively

Figure 3 Low-altitude oblique photograph of an alfalfa field exhibiting complex networks of vegetated crop lines taken on July 19, 2012, in eastern Jo Daviess County. North is to the left. Scale 1 in. = 115 ft (approximate). Areas ST 4 and CL 7, Map 1 T28N, R5E; see Figures A1–A2 and Tables A1–A2 (photograph by S. Panno).

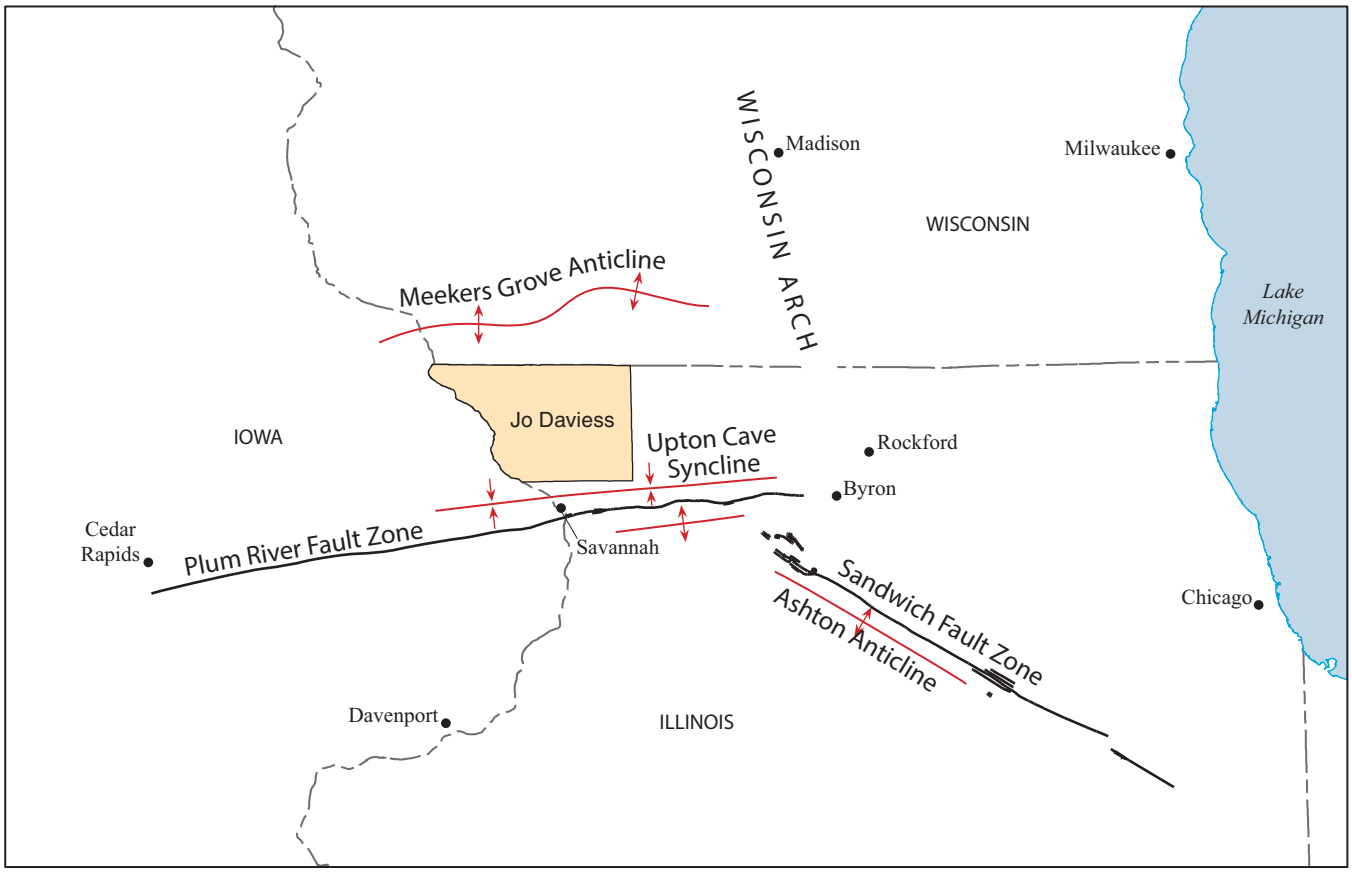

Figure 4 Major structural features in northern Illinois, southern Wisconsin, and eastern Iowa. Scale 1 in. = 35 mi (approximate).

referred to as the Galena-Platteville dolomite (Hackett and Bergestrom 1956; Csallany and Walton 1963). Csallany and Walton (1963) found that the most water-yielding openings occur in the upper one-third of the shallow dolomite aquifer. They stated that some shallow dolomite wells have yields in excess of 1,000 gal/min (3,785 L/min). They also determined that where the Galena-Platteville dolomite is overlain by unconsolidated deposits in northern Illinois, solution activity has enlarged openings, and the Galena-Platteville dolomite yields moderate quantities of water to wells. However, where it is overlain by the Maquoketa Shale, the Galena-Platteville dolomite is a less favorable source of groundwater and yields little water from joints, fissures, and solution cavities. Weibel and Panno (1997) and McGarry (2000) have mapped much of the county area as karst.

Jo Daviess County is situated on the southwest flank of the Wisconsin Arch, a broad north–south-trending crustal uplift that extends through central Wisconsin into north-central Illinois (Figure 4). The regional dip of bedrock within the study area is about 17 ft/mi (3.2 m/km) to the south-southwest (Heyl et al. 1959). Immediately south is the Plum River Fault Zone, a major structural feature that extends from near Cedar Rapids, Iowa, east-northeast for approximately 118 mi (190 km) to near Byron in north-central Illinois (Kolata and Buschbach 1976; Bunker et al. 1985; Figure 4). The zone is up to 1 mi (1.6 km) wide and is composed of largely vertical faults with a cumulative displacement of as much as 400 ft (120 m) to the north near Savanah, Illinois. A syncline flanks the north side, whereas domes and anticlines flank the south side of the fault zone. The Meekers Grove Anticline is situated just north of the study area in southwestern Wisconsin (Figure 4). Away from the Plum River Fault Zone, most faults in the region are small, reverse-bedding-plane normal shear faults with less than 10 ft (<3 m) of displacement (Kolata and Buschbach 1976; Bunker et al. 1985).

The regional southward dip of bedrock within the county is interrupted by complex but very gentle anticlines and synclines in an array that trends northeastward, eastward, or northwestward (Bradbury et al. 1956). These folds consist of linear uplifts and depressions that range from 1 mi (1.6 km) to approximately 30 mi (50 km) in length and have limbs that dip less than 15 degrees. Thrust faults with as much as 50 ft (15 m) of displacement are locally present on the northern flanks of the

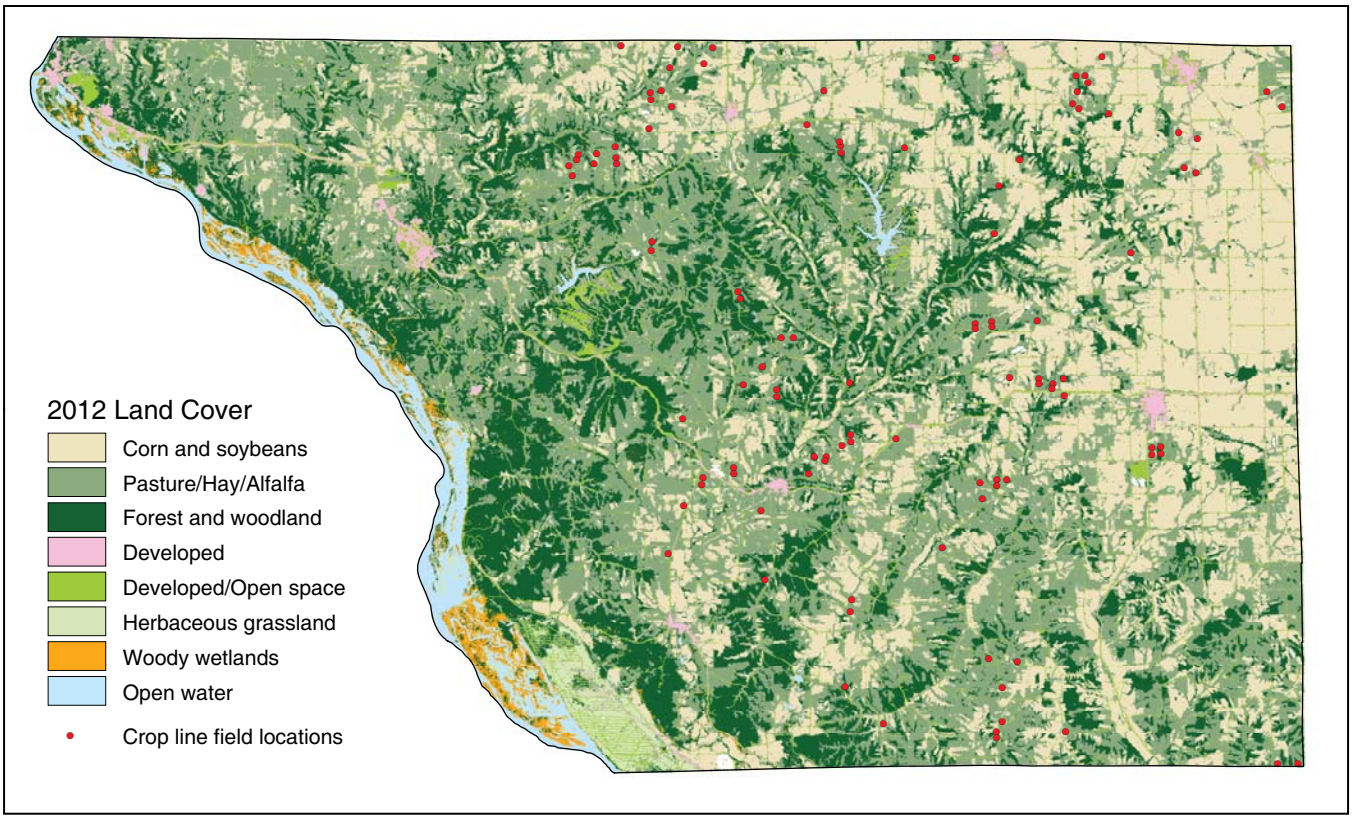

Figure 5 Prevailing land cover for Jo Daviess County in 2012 as interpreted from satellite imagery and ancillary data sources (USDA 2012). Forty percent of the county surface area is devoted to pasture, hay, or alfalfa. Note the correspondence between this land cover type and the occurrence of crop line field locations used for this study. Scale 1 in. = 5.5 mi (approximate).

anticlines (Heyl et al. 1959). Most of the lead and zinc deposits formerly mined in Jo Daviess County were recovered from the solution-enlarged fractures, folds, and faults in the dolomite and limestone of the Platteville Group, the Decorah Subgroup, and the Galena Group (Willman et al. 1946; Willman and Reynolds 1947; Bradbury et al. 1956). Thus, the patterns of surface and underground mine workings reveal fracture patterns in the underlying bedrock.

REMOTE SENSING DATA AND METHODS: AERIAL PHOTOGRAPHY OF VEGETATED CROP LINES

The Mississippi River forms the western border of Jo Daviess County, and stream action from several major tributaries has resulted in a highly dissected landscape containing the greatest local relief [~645 ft (197 m)] of any county in the state. The shallow soil and moderate to steeply sloping land surface are factors limiting the cultivation of row crops, primarily corn and soybeans. Agricultural lands typically account for 90% or more of the surface area in many rural Illinois counties, with corn and soybeans constituting nearly that entire amount (ISGS 2000). Within the study area, these two crops make up only 30% of the total land area, whereas hayfields and pasturelands account for 40% of the county land area (USDA 2012; Figure 5).

Diseased or stressed vegetation is commonly used as an indicator in remote sensing studies to detect and delineate ephemeral phenomena. The 2012 summer drought adversely affected the health and vigor of agricultural crops in Illinois during the entire length of the growing season. Beginning in early June 2012, vegetated crop lines confined mostly to alfalfa hayfields began to manifest as a distinctive landscape feature across the county.

Alfalfa is described by the Soil and Health Library (2012) as

> a long-lived, very deeply rooted perennial. Upon germination, a strong taproot develops rapidly and penetrates almost vertically downward. It often reaches a depth of 1.5 to 1.8 m [~5–6 ft] the first season, 3.0 to 3.6 m [~10–12 ft] by the end of the second year, and may ultimately extend to depths of 6.1 m [20 ft] or more. It is notably a deep feeder.

Consequently, the vigorous root system of alfalfa enabled plants near the bedrock fractures and crevices of the karst aquifer to obtain sufficient moisture and nutrients during the 2012 summer drought to maintain healthy growth. Alfalfa plants forming the vegetated crop lines were taller [~1.5 ft (0.5 m) vs. 0.5 ft (0.15 m)], denser, and greener than adjacent plants in the field, which exhibited stunted and sparse plant growth (Figures 2 and 3).

In contrast, corn and soybean plants possess shallower root systems; therefore, occurrences of vegetated crop lines within these two crops were rare. Corn roots reach depths of approximately 4 ft (1.2 m), with less than 10% of the moisture absorbed by the root system occurring below about 3 ft (1 m; McWilliams et al. 2004). Soybean roots extend to a depth of approximately 4 to 8 ft (1.2 to 2.4 m), with most of the roots being in about the upper 0.5 to 1 ft (0.15 to 0.30 m) of soil (Ransom 2013). Because the deep-rooted alfalfa is a primary hay crop and is the predominant land cover in the study area, it is typically planted on slopes greater than 5% to control soil erosion; thus, the potential for vegetated crop lines to occur across the study area was significantly increased during the 2012 growing season.

The ephemeral nature of the vegetated crop lines, restricted to a relatively brief temporal period during the 2012 growing season, made their detection problematic. Complicating factors were that farm operators typically harvest (alfalfa) hayfields at various times and frequencies during the summer months; therefore, optimal field conditions and subsurface factors were necessary for vegetated crop lines to appear. Because of the large geographic area where vegetated crop lines could potentially appear within agricultural lands (Figure 5), aerial photography was acquired from multiple sources on multiple dates during the period from June to September 2012 for the purpose of mapping their spatial extent (Figures A1 and A2). The U.S. Department of Agriculture collects summer-season aerial photography as part of its nationwide National Agriculture Imagery Program (NAIP), and the annual acquisition period for Illinois NAIP extends from mid-June through August. Although NAIP imagery is of medium resolution [3.3 × 3.3 ft (1 × 1 m), ground sample distance (GSD)] and was acquired for the study area in June during an earlier stage of the drought, vegetated crop lines were nonetheless detectable at several locations (Figure 6a). In July, low-altitude oblique aerial photography for preselected areas was acquired at approximately 984 ft (300 m) above ground level with a handheld digital camera, which yielded some dramatic views of well-developed vegetated crop lines (Figures 3 and 6b).

Using these two remote sensing sources as a guide, the Illinois Department of Transportation (IDOT) Aerial Surveys flew a reconnaissance mission in August 2012 that captured high-resolution vertical aerial photography [0.25 × 0.25 ft (~0.08 × 0.08 m), GSD] of vegetated crop lines for 15 specified locations across the county (see Figure A1 and Table A1). Last, Google aerial photography (unknown GSD) acquired on September 27, 2012, provided the most comprehensive inventory of vegetated crop lines. One hundred twenty-eight locations were identified that exhibited a wide range of vegetated crop line development (see Figure A2 and Table A2).

Using these aerial photography sources, we determined all vegetated crop line features to be evidence of bedrock fractures and crevices (see next section for a discussion), and they were digitized using ArcGIS (http://www.arcgis.com/). The NAIP imagery is orthorectified and is therefore geographic information system (GIS)-ready. Selected frames from the IDOT digitized aerial photography (Figure 7) were manually georeferenced using digital orthophotography acquired in April 2011. The Google aerial photographs were captured in Google Earth (https://www.google.com/earth/; Figures 8 and 9) by using a specialized program, Shape2Earth (http://shape2earthengine.com/shape2earth/Home.html), which transforms the orthgraphic imagery to a georeferenced format. The results of the digitizing yielded 17,855 separate fractures (Figure 10). The original imagery and digitized fractures are documented in the Appendix.

RESULTS AND DISCUSSION

Vegetated Crop Line Fractures and Crevices

Less than approximately 26 ft (8 m) of soil and unconsolidated material overlies the fractured and creviced carbonate bedrock within Jo Daviess County (Riggs and McGarry 2000). Measurements of soil thickness in the areas between the vegetated crop lines at two field locations ranged from approximately 2 to 4 ft (0.6 to 1.2 m). Soil thicknesses immediately over the vegetated crop lines were typically greater than approximately 5 ft (1.5 m). Excavation of the lines revealed that many contained fine-grained sediments, some of which could be the weathering product of Maquoketa Shale. The depth of the fine-grained sediments within the crevices was measured with a Geoprobe System (Salina, Kansas) to be at least 10 ft (3 m) for one crevice examined near a small stream. The drilling retrieved wet, fine-grained sediment, with groundwater draining from the core upon retrieval (T. Prescott, Illinois Natural Resources Conservation Service, personal communication, 2012). The presence of free water within the sediments and the location of the core suggested that the Geoprobe intersected the water table and that water was moving through the crevices, perhaps along piping channels.

A rose diagram summarizing the azimuth orientations for all the vegetated crop lines that were digitized shows a strongly dominant trend oriented east–west, with average azimuths of 95 and 275 degrees, respectively (Figure 10). The azimuths of the subdominant trend are nearly north–south in orientation, thus defining a true orthogonal joint system. These orientations follow trends seen in solution-enlarged crevices exposed in outcrops, road cuts, and quarries (Figure 11; Figure M1B on Map 1), convincing evidence that the vegetated crop lines reflect the fractures and crevices of the Galena Dolomite within the study area. Vegetated crop lines are restricted to soils overlying the Galena Dolomite and Maquoketa Shale because within these areas, the soils are thinnest, land slopes are steeper, and therefore alfalfa is the optimal cover crop for the terrain conditions.

It is also possible that the widths and extent of the vegetated crop lines could be used as a surrogate for the fractures and crevices present on the bedrock surface (Figures 7–9). Vegetated crop lines, coupled with solution-enlarged crevices seen in the bedrock exposures, yield orientations and spacing of fractures and crevices that make up much of the storage capacity and flow paths of the karst aquifer. The vegetated crop lines,

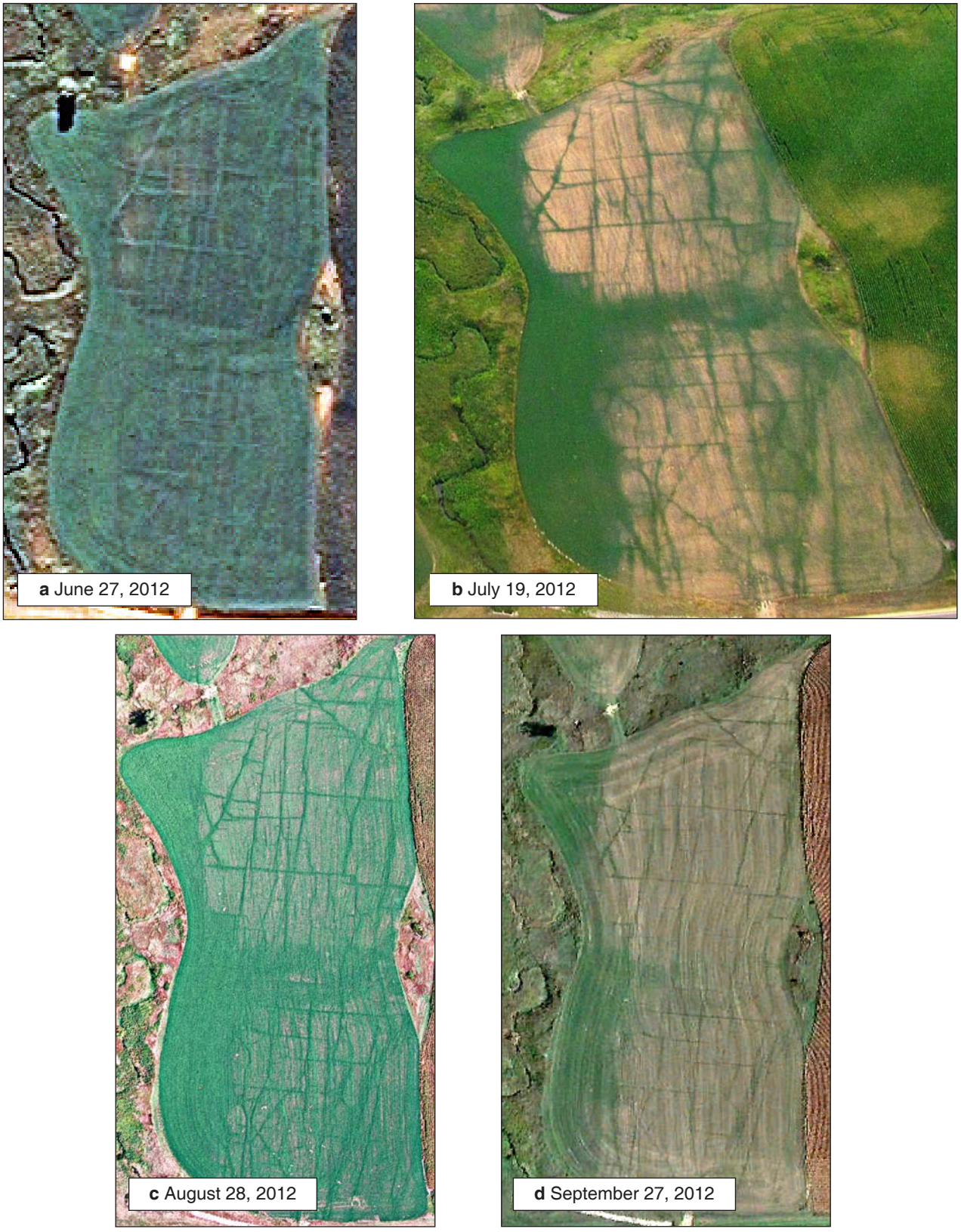

Figure 6 Example of multitemporal remote sensing data sources used to detect and delineate vegetated crop line areas: (a) USDA National Agriculture Imagery Program (NAIP), (b) reconnaissance oblique aerial photography, (c) reconnaissance vertical aerial photography (area ST 4; Map 1 T28–29N, R4–5E; see Figure A1 and Table A1), (d) Google georeferenced vertical aerial photography (area CL 7; Map 1 T28N, R4–5E; see Figure A2 and Table A2). The vegetated networks began appearing in June, became more distinct as the summer drought intensified during July and August, and had largely disappeared by October. North is to the left. Scale for a, c, and d is 1 in. = 225 ft (approximate).

Figure 7 Example of the reconnaissance vertical aerial photography of two alfalfa fields exhibiting pronounced vegetated crop lines acquired on August 28, 2012 (areas ST 10 and CL 48–49; Map 1 T28N, R3–4E; see Figures A1–A2 and Tables A1–A2, respectively). An enlargement of a small portion of the upper field (A) shows in exceptional detail how the alfalfa plants mimic the underlying bedrock fracture and crevice patterns. The more prominent vegetated crop lines shown in (A) average approximately 4 ft (1.2 m) wide, and the varying widths may be indicative of the relative widths of the buried fractures and crevices. North is at the top of the photographs. Scale 1 in. = 250 ft (upper photograph); 1 in. = 50 ft (enlargement). Scales are approximate.

Figure 8 Example of the Google aerial photography of two alfalfa fields exhibiting prominent vegetated crop lines acquired on September 27, 2012 (area CL 24; Map 1 T29N, R4E; see Figure A2 and Table A2). Field excavation in the upper field at the location of the yellow dot revealed a bedrock crevice about 2 in. (5 cm) wide at a depth of approximately 3 ft (1 m), along with an alfalfa tap root embedded in the crevice. The vegetated crop lines visible in this aerial photograph average from 2 to 3 ft (0.6 to 1.0 m) to approximately 6 ft (2 m) in width. North is at the top of the photograph. Scale 1 in. = 115 ft (approximate).

Figure 9 Example of the Google aerial photography of an alfalfa field exhibiting pronounced vegetated crop lines acquired on September 27, 2012. The curvilinear structures within the field are permanent conservation terraces, which are positioned perpendicularly to the prevailing slope to impede erosion. The area is located immediately adjacent to Jo Daviess County in southern Wisconsin (area CL 20; Map 1 T1N, R4E; see Figure A2 and Table A2). The vegetated crop lines visible in this aerial photograph average about 4 to 6 ft (1.2 to 2 m) in width. North is at the top of the photograph. Scale 1 in. = 270 ft (approximate).

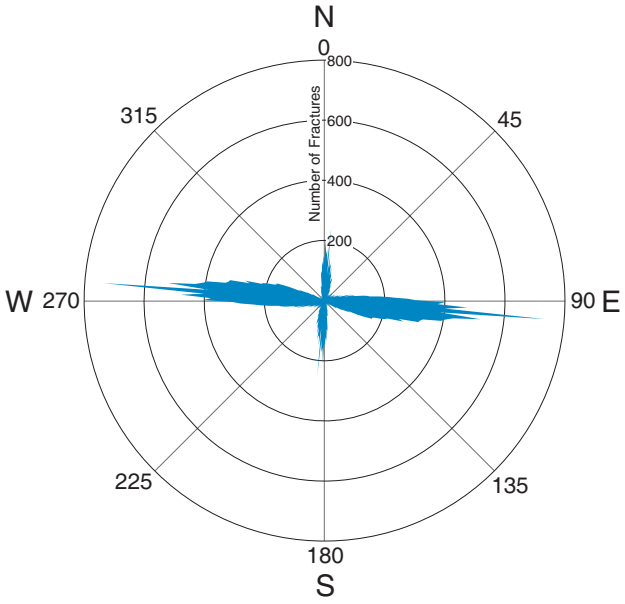

Figure 10 Rose diagram showing the azimuth orientations calculated for 17,855 vegetated crop line fractures digitized from the georeferenced aerial photography locations shown on Map 1 and in Figure A2 and Table A2. The strongly dominant trend is oriented east–west, with average azimuths of 95 and 275 degrees, respectively. The azimuth of the subdominant trend is nearly north–south in orientation.

Figure 11 Example of the Google vertical aerial photography acquired on September 27, 2012 (area CL 146; Map 1 T29N, R2E; see Figure A2 and Table A2). The aerial photograph shows a small abandoned quarry at (A) with exposed bedrock fractures and crevices on the quarry floor. Their orientations correspond to the vegetated crop lines visible at (B) and (C), and are direct evidence that the vegetated crop lines are an accurate reflection of the subsurface bedrock fractures and crevices. North is at the top of the photograph. Scale 1 in. = 205 ft (approximate).

coupled with previous work by Bradbury et al. (1956), Heyl et al. (1959), and Panno et al. (2015) describing the fractures and crevices in road cuts and quarries in the study area, yield spacing of the fractures and crevices that make up much of the connected porosity and storage capacity and many of the flow paths of the Galena Dolomite karst aquifer.

Alignments of Silurian Sinkholes

Analysis of LiDAR elevation data revealed numerous cover-collapse sinkholes in western Jo Daviess County developed in the unconsolidated deposits overlying the Silurian dolomite (Figure 12 and Map 1). The cover-collapse sinkholes that could be delineated are oriented en echelon in an approximately east–west orientation and have average azimuths of 105 and 285 degrees, respectively (Figure A3 and Table A3). This trend is within 10 degrees of the dominant orientation of the vegetated crop lines (Figure 10), additional evidence the vegetated crop lines are an accurate reflection of the fractures and crevices of the underlying bedrock within the study area.

Field examination of these areas revealed solution-enlarged crevices and small caves in addition to sinkholes. Karst features present in the western part of Jo Daviess County in Silurian dolomite include relatively large crevices or cutters in exposures and road cuts (Figure 13) as well as cover-collapse sinkholes in fine-grained sediment overlying the dolomite. Solution-enlarged crevices in the Silurian dolomite can be up to approximately 3 ft (1 m) in width and are numerous. Sinkholes in this area are roughly circular in plan view, typically bowl-shaped, approximately 6 to 23 ft (2 to 7 m) deep, and approximately 60 to 100 ft (20 to 30 m) in diameter based on measurements from LiDAR elevation data. Several of these sinkholes initially seen in aerial photographs were documented by Weibel and Panno (1997) and Panno et al. (1997). Weibel and Panno (1997) and Panno et al. (1997) reported them to be collapse features with no evidence of waste piles that would suggest excavations (Figure 12). Consequently, the features were interpreted as sinkholes and not as small-scale mining operations following veins of ore minerals. Approximately 10 of these cover-collapse sinkholes have been examined in the field, and it is possible a few could be related to adjacent large-scale mining operations (e.g., Touseull and Rich 1980).

Although a large cover-collapse sinkhole area underlain by Silurian dolomite in the southwestern corner of Jo Daviess County is near mining operations, the ore deposits in this area were primarily within the deeper dolomite of the Galena Group underlying the Silurian dolomite and Maquoketa Shale. Therefore, features identified as cover-collapse sinkholes in sediment overlying the Silurian dolomite are typically not related to mining operations. Road cuts in the area between approximately 3 and 5 mi (5 and 8 km) to the east reveal that these aligned sinkholes probably formed along almost east–west-trending crevices that range from approximately 1.5 to 3 ft (0.5 to 1 m) in width (Figure 13). The depth of the crevices is at least approximately 20 ft (6 m) from the land surface, as seen in road cuts. The collapse of sediment into these large crevices probably created the sinkholes and associated lineaments observed in the imagery. In addition, it is possible that large blocks of Silurian dolomite on ridges could have separated along crevices and slowly migrated downhill on the underlying shale. This would have dilated existing crevices even more, thereby creating additional aligned collapse features (D. Mikulic, Illinois State Geological Survey, personal communication, 2014). In addition, strike-slip shearing with an extensional component would have enlarged fractures, making them highly prone to further widening by solution.

Alignments from Lead-Zinc Mining Operations

The Upper Mississippi Valley (UMV) mining district lies within the Driftless Area of northwestern Illinois and includes the study area, southwestern Wisconsin, and northeastern Iowa. From the early 19th century into the middle of the 20th century, the UMV mining district was one of America's leading producers of lead and zinc. These ores, primarily galena and sphalerite, were concentrated along near-vertical solution-enlarged fractures and shear joints that extend up to 2 mi (3.2 km) in length within middle Ordovician-age limestone and dolomite, primarily within the Galena Group. The crevice deposits trended roughly east–west along the southwestern flank of the Wisconsin Arch (Bradbury 1959; Figure 4). The UMV mining district is bounded by first-order structural features that include the Illinois Basin to the south, the Wisconsin Arch to the north, and the Forest City Basin to the west. The geology of the UMV mining district and its ore deposits has been summarized by Heyl et al. (1959) and Bradbury (1959). Formation of the ore deposits has been tied to the Alleghanian/Ouachita Orogeny that initiated a regional-scale brine migration across the Midwest. The timing of ore mineralization is estimated to be approximately 270 Ma before present (Brannon et al. 1992). Bethke (1986) suggested that the ore-forming brines probably originated from the Illinois Basin and migrated along a gravity-driven gradient toward the north. Recent data by Panno et al. (2013) on chlorine/bromine (Cl/Br) ratios of fluid inclusions in sphalerite samples from the UMV district suggest that if the Illinois Basin was the source of the ore-forming brines, they probably originated from or migrated through Pennsylvanian-age strata.

Mining in Jo Daviess County extends back to the Native Americans, who extracted galena for ornamental use and later in the late 1600s for trading with the French. Lacking metal tools, explosives, and smelting technology, Native Americans were undoubtedly limited in their mining techniques to picking crystals out of surface exposures. Settlers moving into the area during the 1830s forcibly took over lands from the Native Americans with the assistance of the U.S. Government (Jelatis 2009). Underground mining commenced soon after initial settlement, and by 1845, the city of Galena, Illinois, produced 80% of the lead in the United States—the last mine closed in 1979 (Mining History Association 2013). Heyl et al. (1978) described early mining in the area as follows:

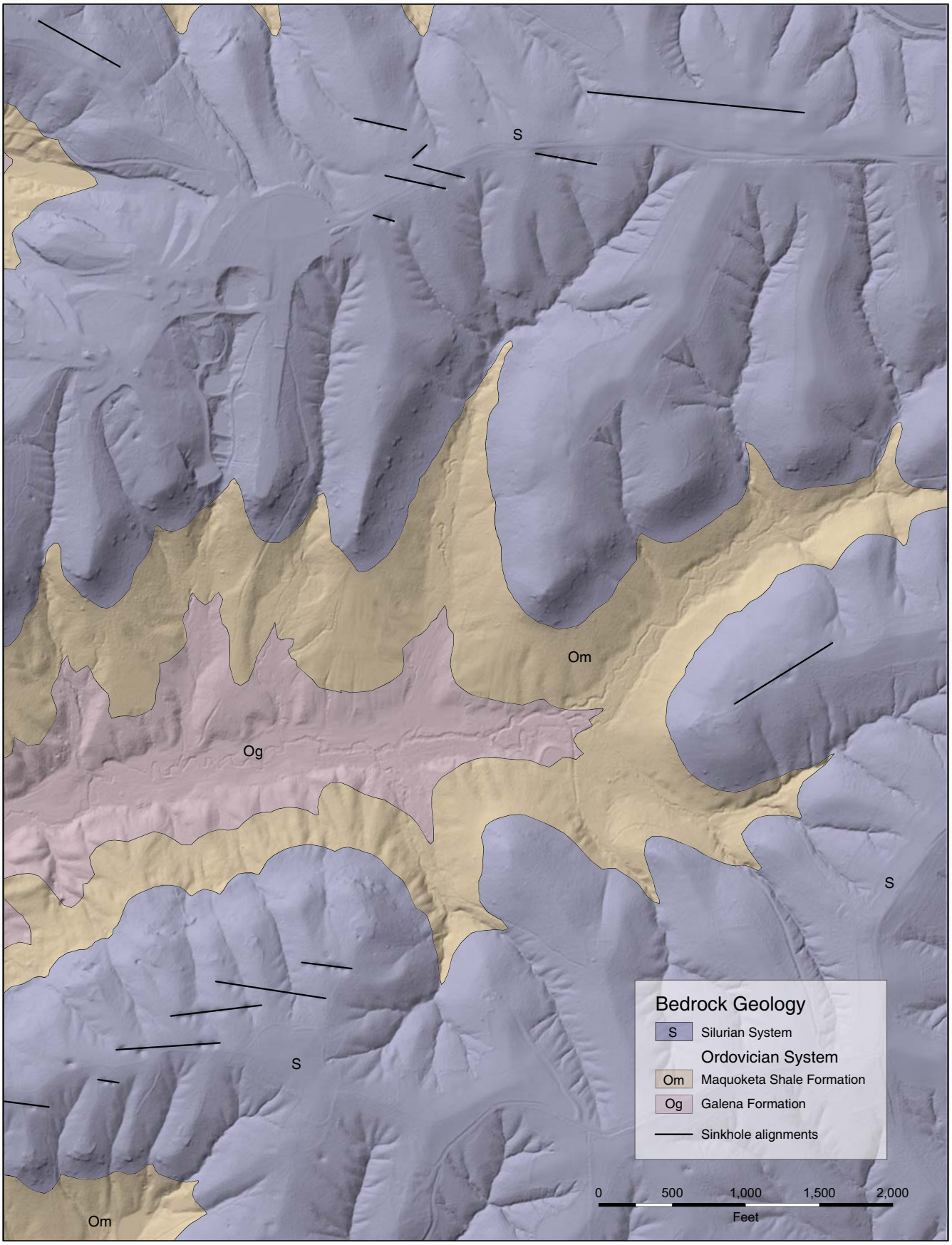

Figure 12 Shaded relief model produced from 2008 LiDAR bare-earth elevation data showing aligned sinkholes in highly fractured and creviced Silurian-age dolomite (areas S 3–5 and S 8; Map 1 T27N, R1E; Figure A3 and Table A3). The dominant trend of the sinkhole alignments (black lines) corresponds to the dominant orientation of the vegetated crop lines (Figure 10). North is at the top of the image. Scale 1 in. = 1,000 ft (approximate).

Figure 13 Road cut exposure of Silurian-age dolomite near Elizabeth, Illinois, in Jo Daviess County. Solution-enlarged crevices in the Silurian dolomite can be up to approximately 3 ft (1 m) in width (photograph by S. Panno).

> Production was largely from "float" deposits formed by weathering of sulfide veins that left concentrations of residual galena on hillside bedrock overlain by varying thicknesses of residual soil. The miners would dig a pit to bedrock, extending outward in all directions, dragging the galena to the center. The mining limit of each pit was soon reached, and then the miners simply moved a short distance away and dug another pit. This system of "suckering" produced the pock-marked hillsides so common in the district. (p. 4)

Because ore emplacement was the result of mineralization along preexisting fractures and crevices, the lines of sucker holes (diggings) provide a means of measuring the orientation of ore-bearing veins; therefore, fracture trends can be delineated within the Galena Dolomite that existed at the time of ore mineralization (ca. 270 Ma before present; Brannon et al. 1992). Mine diggings in Jo Daviess County possess a dominant trend oriented west to east, and a lesser north-to-south trend, consistent with the orientations of the vegetated crop lines (Figure 10).

Present-day remnants of large-scale mining operations are visible on the ground as waste piles and mine openings at the base of bluffs. The mining operations and their scars on the landscape were first mapped by Grant and Perdue (1908) on the Millbrig Quadrangle, which included the Vinegar Hill Mine diggings (Figure 14). Subsequent detailed mapping of these diggings by the Vinegar Hill Mining Company revealed aligned diggings that typically followed veins of ore minerals (Cox 1914). Examination of the LiDAR elevation data revealed abundant evidence of mining disturbances throughout the county (see Map 1 and Figure A4 and Table A4), including numerous alignments of mine diggings. An overlay of a map of the Vinegar Hill diggings reported by Cox (1914) combined with a LiDAR shaded relief model for the same geographic area illustrates a high degree of accuracy, as well as evidence of additional diggings that appear to postdate the 1914 Cox map (Figures 15–17). Analysis of the mine digging alignments digitized from the LiDAR elevation data shows an almost east–west dominant trend, with average azimuths of 101 and 281 degrees, respectively, consistent with those of the vegetated crop lines (Figure 10) and the aligned sinkholes developed in the Silurian dolomite (see Figure A3 and Table A3)—further evidence that the vegetated crop lines are a surrogate for fractures and crevices in the underlying bedrock.

Tectonic Implications of Bedrock Fractures

Bedrock throughout the Midcontinent of the United States, including northern Illinois, exhibits vertical fractures or

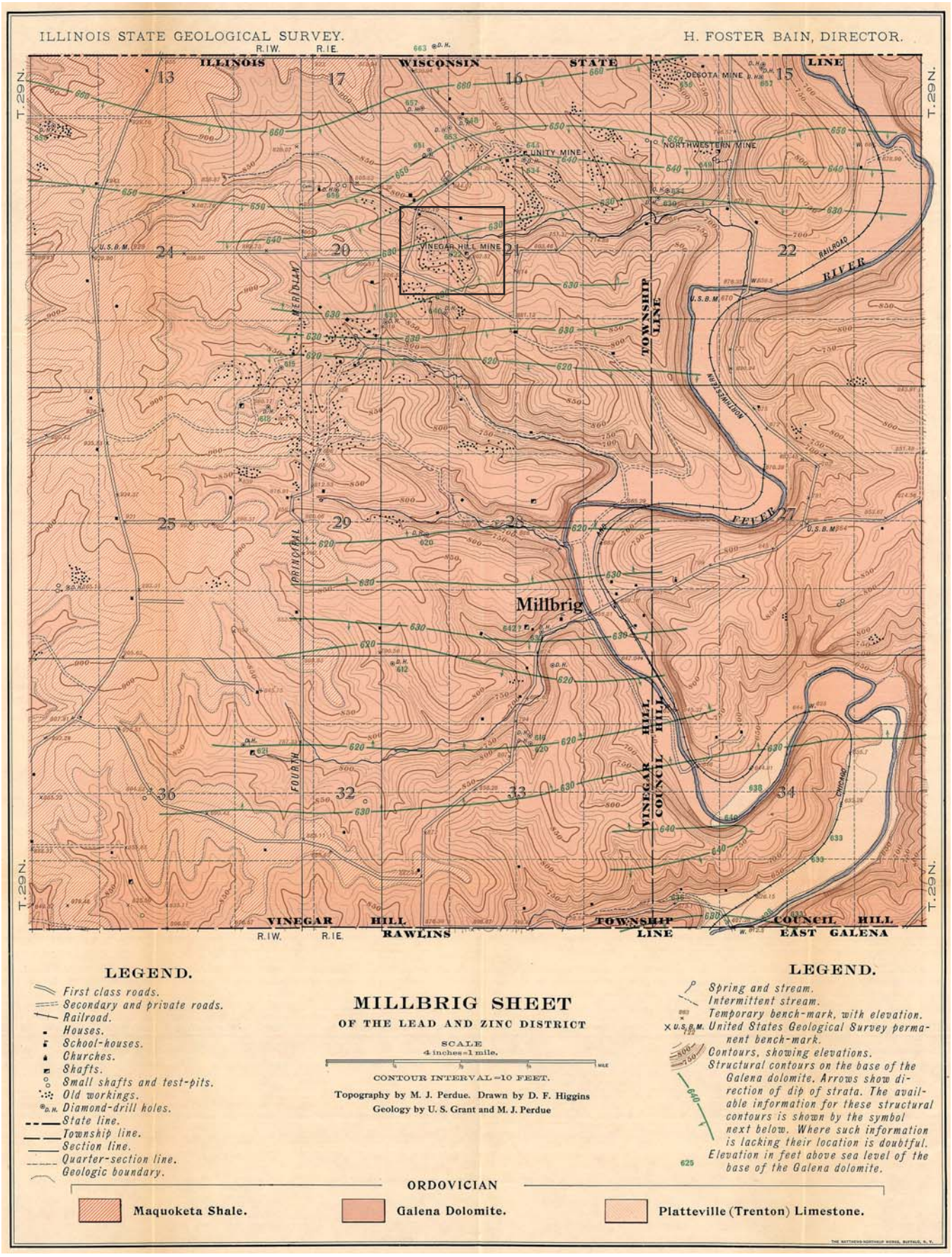

Figure 14 Millbrig sheet geologic map showing the distribution of lead and zinc diggings in 1908 for an area north of Galena, Illinois, in northwestern Jo Daviess County. The outlined area is the location of the Vinegar Hill Mine and diggings (Grant and Perdue 1908; compare with Figures 15–17). Map has been reduced to 50% of its original size.

Figure 15 Vertical aerial photograph acquired in April 2011 showing the original Vinegar Hill Mine site in northwestern Jo Daviess County (see also Figure 14 for location). Many of the diggings are now obscured by woody vegetation. The light-toned area represents the spoils from underground mining operations (compare with Figures 16 and 17). North is at the top of the photograph. Scale 1 in. = 333 ft (approximate).

joints. These fractures or joints have long been observed in the numerous mines, quarries, road cuts, and natural exposures in northwestern Illinois. Many of the vertical fractures are traceable horizontally for 2 mi (3.2 km) or more (Heyl et al. 1959) and have been observed at depths of 5,000 ft (1,524 m) in exploratory drill holes in adjacent Stephenson County (Haimson and Doe 1983). In Jo Daviess County, the predominant fracture trends, as inferred from the vegetated crop lines, are oriented nearly east–west, with average azimuths of 95 and 275 degrees, respectively. The secondary joint trend is oriented nearly north–south (Figure 10). Locally, the average trends vary by as much as 10 degrees (Figure 18), but overall, they are consistent with the bedrock fracture orientations observed in the zinc-lead district of northwestern Illinois and southwestern Wisconsin (Heyl et al. 1959); in Boone and Winnebago Counties, Illinois (McGarry 2000); and in northeastern Illinois and northern Indiana (Foote 1982; Figure 19). One of the areas of greatest divergence in the trend of fractures and crevices occurs in the northeastern part of Jo Daviess County (area B in Figure 18). Here, the primary fracture trend is oriented almost east–west at average azimuths of 85 degrees, and the secondary fractures are oriented slightly west of north at 175 degrees.

Field and laboratory results indicate that regional fracture systems form parallel to maximum compressive

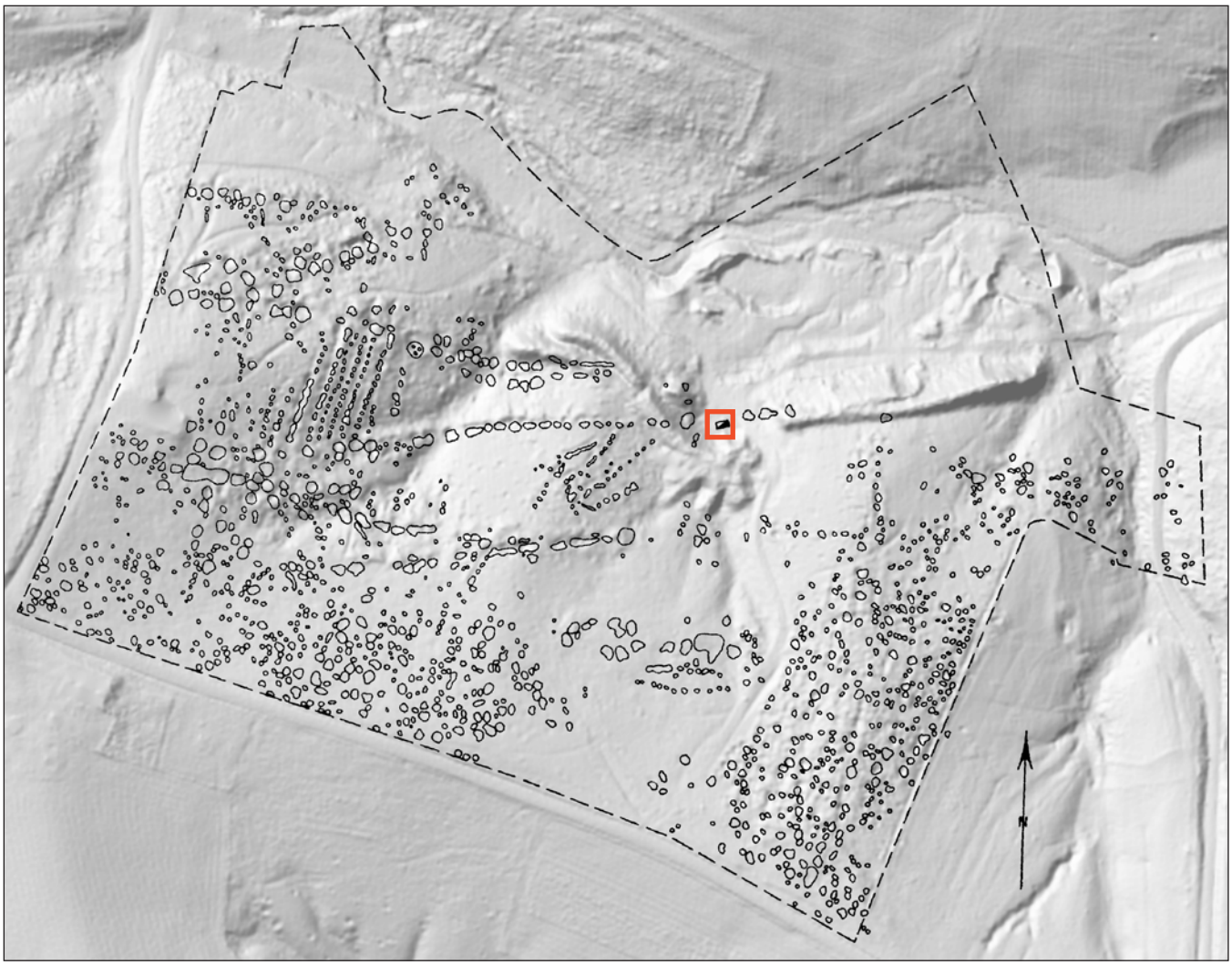

Figure 16 Engineering drawing of the Vinegar Hill Mine diggings (black outlines) as they appeared in 1914, superimposed on 2008 LiDAR bare-earth elevation data (in the region of area D 5, Map 1 T29N, R1E; see Figure A4 and Table A4). Each of the areas represents an excavation from mining lead and zinc (from Cox 1914). The red outline marks the location of the mine shaft (compare with the aerial photograph in Figure 15 and the LiDAR shaded relief model in Figure 17. North is at the top of the image. Scale 1 in. = 333 ft (approximate).

stress trajectories, making fracture orientations highly sensitive indicators of paleostress fields (Hubbert and Willis 1957; Engelder and Geiser 1980). This has led several authors to suggest that the dominant northwest–southeast-trending fractures in the Midcontinent (Figure 19) were caused by far-field stress transmission from the Appalachian fold-and-thrust belt during the late Paleozoic Alleghanian Orogeny (Apotria et al. 1994; McGarry 2000). This event corresponds in age to the widespread structural deformation that occurred in the Midcontinent beginning in Late Mississippian (Chesterian) time, peaking during the Early Pennsylvanian (Morrowan and Atokan), and continuing intermittently through the remainder of Pennsylvanian time (Kolata and Nelson 1991). The west–northwest- and east–southeast-trending fractures in the zinc-lead district of northwestern Illinois and southwestern Wisconsin contain sphalerite that has been dated by rubidium-strontium (Rb-Sr) methods at 270 Ma (Brannon et al. 1992), indicating that these fractures were already formed by early Permian time. Supporting evidence for northwest-oriented far-field stress transmission during the late Paleozoic Alleghanian Orogeny is seen in layer-parallel shortening that is preserved by mechanically twinned calcite in carbonate rocks of the Midcontinent (Craddock et al. 1993). Accordingly, the shortening strain magnitudes and inferred calcite twinning differential stress magnitudes decrease exponentially away from the orogenic front.

The origin of the secondary north-trending fractures in the study area is not entirely clear. The fact that these fractures contain many fewer zinc and

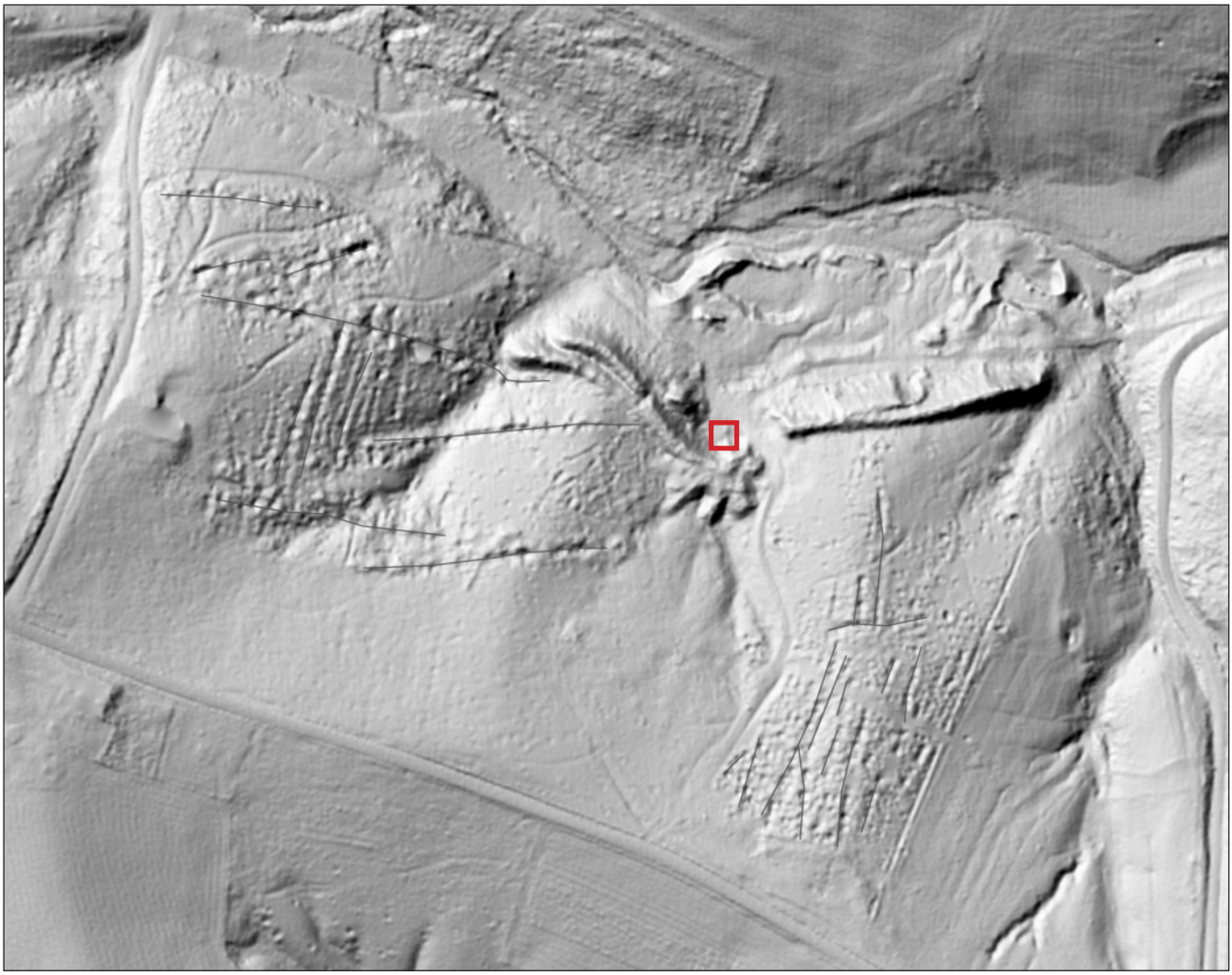

Figure 17 Shaded relief model produced from 2008 LiDAR bare-earth elevation data (in the region of area D 5, Map 1 T29N, R1E; see Figure A4 and Table A4). The excavations, or diggings, shown on this image range in depth from approximately 1 to 5 ft (0.3 to 1.5 m). The major digging alignments (thin black lines) are consistent with the orientations of the vegetated crop lines (Figure 10). The red outline marks the location of the mine shaft (compare with Figures 15 and 16). North is at the top of the image. Scale 1 in. = 333 ft (approximate).

lead deposits (Heyl et al. 1959) than do the east-trending fractures (see Figure 10 and inset rose diagram in Figure 18) suggests that the north-trending fractures formed after early Permian time. The coincidence in orientation of these fractures and the contemporary orientation of maximum horizontal compression stress suggests that tensile stresses associated with current rifting along the mid-Atlantic ridge may have caused the fractures (Engelder 1982; Foote 1982; Hancock and Engelder 1989; Gross and Engelder 1991; Apotria et al. 1994; McGarry 2000). Examination of the tectonic forces responsible for the fractures and crevices within the study area provides insights into the character and geometry of the important karst aquifer that provides potable groundwater to Jo Daviess County.

CONCLUSIONS

An investigation of 17,855 vegetated crop lines that appeared during the extreme drought in the summer of 2012 has provided a new information source for investigating and characterizing the karst aquifer within Jo Daviess County, Illinois. The vegetated crop lines typically occurred in alfalfa hayfields in locations where the unconsolidated materials overlying the bedrock surface are approximately 2 to 4 ft (~0.6 to 1.2 m) in thickness (author's field observations).

The widths, orientations, and distance of separation of the vegetated crop lines were analyzed. It was determined they possess characteristics similar to those of solution-enlarged crevices exposed in outcrops, road cuts, and quarries within the county. A rose diagram summarizing the azimuth orientations for the

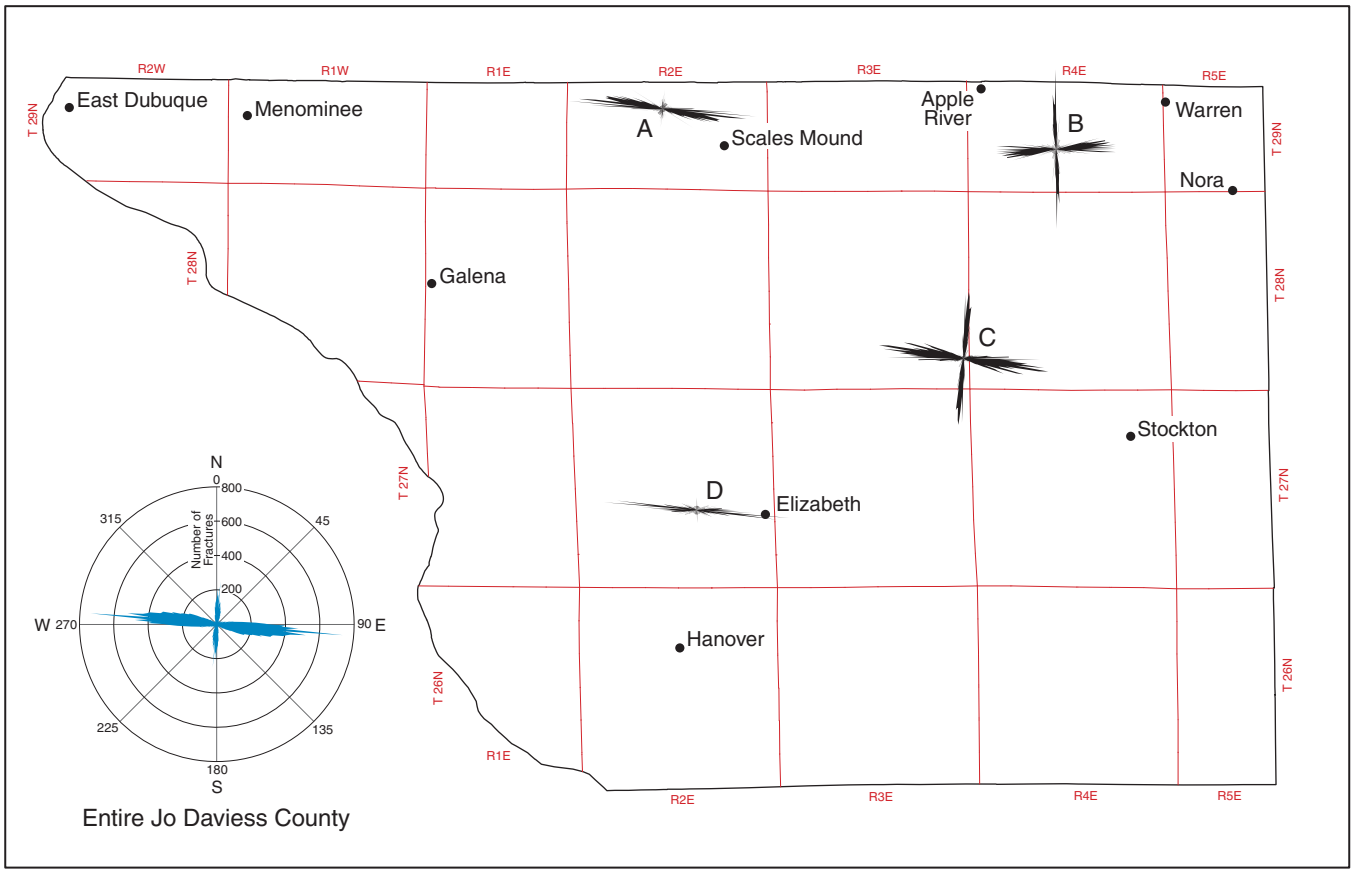

Figure 18 Rose diagrams showing azimuth orientations for fractures measured at four locations (A,B,C, and D) in Jo Daviess County, Illinois. Fracture orientations at localities A, C, and D are generally similar to the overall pattern for Jo Daviess County as shown in the inset rose diagram. However, locality B displays a slight, approximately 15-degree counterclockwise shift in both the dominant west-northwest–east-southeast and subdominant nearly north–south trends. Scale 1 in. = 6 mi (approximate).

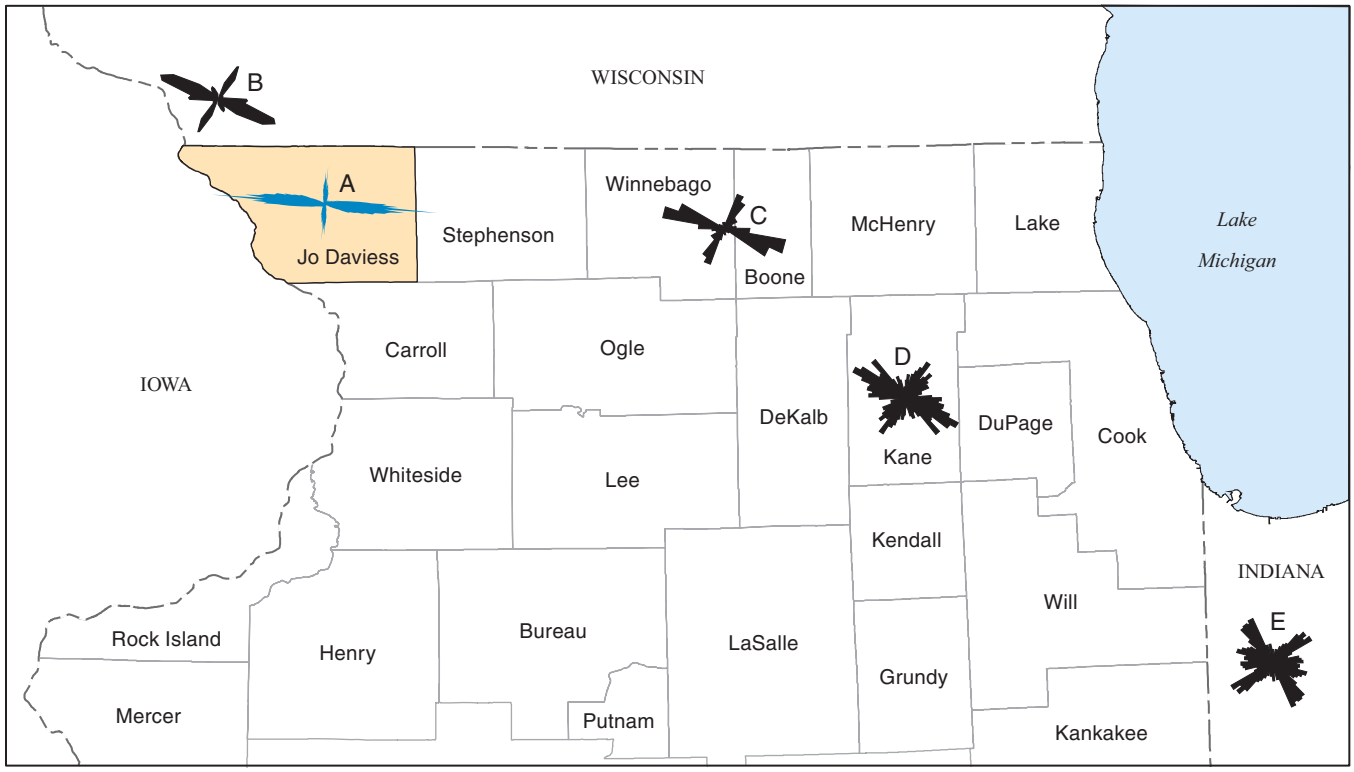

Figure 19 Rose diagrams showing dominant and subdominant fracture trends from (A) this study, (B) Heyl et al. (1959), (C) McGarry (2000), and (D, E) Foote (1982). Scale 1 in. = 30 mi (approximate).

vegetated crop lines shows a dominant trend oriented almost east–west at average azimuths of 95 and 275 degrees, respectively. Azimuths of the subdominant trend are almost north–south in orientation (Figure 10; also see Map 1).

Additionally, analysis of LiDAR elevation data of digitized fractures and crevice patterns associated with abandoned lead and zinc mine diggings, and alignments of cover-collapse sinkholes showed that the orientations of these features are consistent with those of fractures and crevices observed in exposures throughout the county and with the vegetated crop lines.

These fractures and crevices probably formed contemporaneously with the Appalachian fold-and-thrust belt during the late Paleozoic Alleghanian Orogeny and are the predominant host of the zinc-lead ore deposits in the Driftless Area. The origin of the subdominant almost north–south-trending fractures and crevices is not so clear, and the paucity of ore mineralization suggests that the fractures formed after early Permian time, possibly because of current rifting along the Mid-Atlantic Ridge.

The results of this investigation confirm that the vegetated crop lines identified and digitized from the multidate aerial photography and LiDAR elevation data can be used as direct surrogates for mapping the fracture and crevice patterns on the buried carbonate bedrock surface. Digitized data sets constituting the vegetated crop lines, and alignments of cover-collapse sinkholes and mine diggings can be used to better characterize the geometry and character of the karst aquifer within the Driftless Area of northwestern Illinois.

ACKNOWLEDGMENTS

The authors thank Matthew Altschuler of Jo Daviess County for notifying the authors of the appearance of vegetated crop lines in the summer of 2012, and Jeff Kromer of Mount Carroll, Illinois, for the generous donation of his time, skills, and aircraft to capture reconnaissance aerial photography over Jo Daviess County. The authors also thank Walton Kelly of the Illinois State Water Survey for his assistance in the field and insightful observations, and Amy Eller of IDOT for contributing Aerial Survey Division resources to acquire the vertical aerial photography in a timely manner.

The authors express their sincere thanks to the staff at the ISGS who were responsible for the preparation of the maps, figures, and illustrations; scientific reviews and editing; and production of this publication: Jennifer Carrell, Jane Johnshoy Domier, Michael Knapp, Richard Berg, Steven Brown, Brandon Curry, David Larson, John Nelson, and Susan Krusemark.

REFERENCES

Apotria, T., C.J. Kaiser, and B.A. Cain, 1994, Fracturing and stress history of the Devonian Antrim Shale, Michigan Basin, *in* P.P. Nelson, and S.C. Laubach, eds., Rock mechanics models and measurements: Challenges from industry: Proceedings of the 1st North American Rock Mechanics Symposium: Rotterdam, Netherlands, A.A. Balkema, p. 809–816.

Bethke, C.M., 1986, Hydrogeologic constraints on the genesis of the Upper Mississippi Valley mineral district from Illinois Basin brines: Economic Geology, v. 81, p. 233–249.

Bradbury, J.C., 1959, Crevice lead-zinc deposits of northwestern Illinois: Illinois State Geological Survey, Report of Investigations 210, 49 p.

Bradbury, J.C., R.M. Grogan, and R.J. Cronk, 1956, Geologic structure map of the northwestern Illinois zinc-lead district: Illinois State Geological Survey, Circular 214, 7 p.

Brannon, J.C., F.A. Podosek, and R.K. McLimans, 1992, Alleghenian age of the Upper Mississippi Valley zinc-lead deposits determined by Rb-Sr dating of sphalerite: Nature, v. 356, p. 509–511.

Bunker, B.J., G.A. Ludvigson, and B.J. Witzke, 1985, The Plum River Fault Zone and the structural and stratigraphic framework of eastern Iowa: Iowa Geological Survey, Technical Information Series 13, 123 p.

Cox, G.H., 1914, Lead and zinc deposits of northwestern Illinois, Illinois State Geological Survey, Bulletin 21, 120 p.

Craddock, J.P., M. Jackson, B.A. van der Pluijm, and R.T. Versical, 1993, Regional shortening fabrics in eastern North America: Far-field stress transmission from the Appalachian-Ouachita orogenic belt: Tectonics, v. 12, p. 257–264.

Csallany, S., and W.C. Walton, 1963, Yields of shallow dolomite wells in northern Illinois: Illinois State Water Survey, Report of Investigations 46, 43 p.

Engelder, T., 1982, Is there a genetic relationship between selected regional joints and the contemporary stress within the lithosphere of North America? Tectonics, v. 1, p. 161–177.

Engelder, T., and P. Geiser, 1980, On the use of regional joint sets as trajectories of paleostress fields during the development of the Appalachian Plateau, New York: Journal of Geophysical Research, v. 85, p. 6319–6341.

Foote, G.R., 1982, Fracture analysis in northeastern Illinois and northern Indiana: University of Illinois at Urbana-Champaign, M.S. thesis, 192 p.

Ford, D.C., and P.W. Williams, 1992, Karst geomorphology and hydrology: New York, Chapman and Hall, p. 1.

Grant, U.S., and M.J. Perdue, 1908, Millbrig sheet of the lead and zinc district of northern Illinois: Illinois State Geological Survey, Bulletin 8, p. 335–343.

Gross, M.R., and T. Engelder, 1991, A case for neotectonic joints along the Niagara Escarpment: Tectonics, v. 10, p. 631–641.

Hackett, J.E., and R.E. Bergstrom, 1956, Groundwater in northwestern Illinois: Illinois State Geological Survey Division, Circular 207, 25 p.

Haimson, B.C., and T.W. Doe, 1983, State of stress, permeability, and fractures in the Precambrian granite in northern Illinois: Journal of Geophysical Research, v. 88, p. 7355–7371.

Hancock, P.L., and T. Engelder, 1989, Neotectonic joints: Geological Society of America Bulletin, v. 101, p. 1197–1208.

Heyl, A.V., A.F. Agnew Jr., E.J. Lyons, and C.H. Behre Jr., 1959, The geology of the Upper Mississippi Valley zinc-lead district: U.S. Geological Survey, Professional Paper 309, 310 p.

Heyl, A.V., W.A. Broughton, and W.S. West, 1978, Geology of the Upper Mississippi Valley base-metal district: University of Wisconsin-Extension, Geological and Natural History Survey, Information Circular 16, 45 p.

Hubbert, M.K., and D.D. Willis, 1957, Mechanics of hydraulic fracturing: Transactions of AIME, v. 210, p. 153–168.

Illinois State Geological Survey (ISGS), 2000, Land cover data for Illinois: Illinois State Geological Survey, Illinois, Geospatial Data Clearinghouse http://www.isgs.uiuc.edu/nsdihome/webdocs/landcover/index.html (accessed June 10, 2015).

Jelatis, V., 2009, An inflammable region: Indians, Anglo-Americans, and lead mining in northwestern Illinois, 1788–1832: Illinois History Teacher, v. 15, no. 2, p. 2–10.

Kolata, D.R., and T.C. Buschbach, 1976, The Plum River Fault Zone of northwestern Illinois: Illinois State Geological Survey, Circular 491, 20 p.

Kolata, D.R., and W.J. Nelson, 1991, Tectonic history of the Illinois Basin, *in* M.W. Leighton, D.R. Kolata, D.F. Oltz, and J.J. Eidel, eds., Interior cratonic basins: Tulsa, Oklahoma, American Association of Petroleum Geologists, Memoir 51, p. 263–285.

McGarry, C.S., 2000, Regional fracturing of the Galena-Platteville aquifer in Boone and Winnebago Counties, Illinois: Geometry, connectivity and tectonic significance: University of Illinois at Urbana-Champaign, M.S. thesis, 209 p.

McWilliams, D.A., D.R. Berglund, and G.J. Endres, 2004, Soybean growth and management: Quick guide: North Dakota State University, Publication A-1174, http://www.ag.ndsu.edu/pubs/plantsci/rowcrops/a1174/a1174.pdf (accessed June 10, 2015).

Mining History Association, 2013, History of the Upper Mississippi Valley zinc-lead mining district: Canon City, Colorado, Mining History Association Annual Conference, June 6–9, 2013, Galena, Illinois, http://www.mininghistoryassociation.org/GalenaHistory.htm (accessed June 10, 2015).

Nelson, J.W., 1995, Structural features in Illinois: Illinois State Geological Survey, Bulletin 100, 57 p.

Panno, S.V., K.C. Hackley, R.A. Locke, I.G. Krapac, B. Wimmer, A. Iranmanesh, and W.R. Kelly, 2013, Formation waters from Cambrian-age strata, Illinois Basin, USA: Constraints on their origin and evolution based on halide composition: Geochimica et Cosmochimica Acta, v. 122, p. 184–197.

Panno, S.V., D.E. Luman, W.R. Kelly, T.H. Larson, and S.J. Taylor, 2015, Karst terrains of northwestern Illinois' Driftless Area, Jo Daviess County: Illinois State Geological Survey, Circular 586.

Panno, S.V., C.P. Weibel, and W.B. Li, 1997, Karst regions of Illinois: Illinois State Geological Survey, Open File 1997-2, 42 p.

Quinlan, J.F., P.L. Smart, G.M. Schindel, E.C. Alexander Jr., A.J. Edwards, and A.R. Smith, 1991, Recommended administrative/regulatory definition of karst aquifer, principles of classification of carbonate aquifers, practical evaluation of vulnerability of karst aquifers, and determination of optimum sampling frequency at springs, *in* Proceedings of the Third Conference on Hydrogeology, Ecology, Monitoring, and Management of Ground Water in Karst Terranes: U.S. Environmental Protection Agency and Association of Ground Water Scientists and Engineers, p. 573–635.

Ransom, J., 2013, Corn growth and management: Quick guide: North Dakota State University, Publication A-1173, http://www.ag.ndsu.edu/pubs/plantsci/crops/a1173.pdf (accessed June 10, 2015).

Riggs, M.H., and C.S. McGarry, 2000, Map showing thickness of Quaternary deposits, Jo Daviess County, Illinois: Illinois State Geological Survey, Open File 2000-8c, 1 sheet.

Soil and Health Library, 2012, Chapter 13: Root habits of alfalfa, http://www.soilandhealth.org/01aglibrary/010139fieldcroproots/010139ch13.html (accessed June 10, 2015).

Touseull, J., and C. Rich Jr., 1980, Documentation and analysis of a massive rock failure at the Bautsch Mine, Galena, IL: U.S. Bureau of Mines, Report of Investigation 8453, 49 p.

U.S. Department of Agriculture (USDA), National Agricultural Statistics Service, Research and Development Division, Geospatial Information Branch, Spatial Analysis Research Section, 2012, 2012 Illinois cropland data layer, http://www.nass.usda.gov/research/Cropland/Release/index.htm (accessed June 10, 2015).

Weibel, C.P., and S.V. Panno, 1997, Karst terrains and carbonate bedrock of Illinois: Illinois State Geological Survey, Illinois Map Series 8, 1:500,000.

White, W.B., 1988, Geomorphology and hydrology of karst terrains: New York, Oxford University Press, 464 p.

Williams, P.W., 2008, The role of the epikarst in karst and cave hydrogeology: A review: International Journal of Speleology, v. 37, p. 1–10.

Willman, H.B., and R.R. Reynolds, 1947, Geological structure of the zinc-lead district of northwestern Illinois: Illinois State Geological Survey, Report of Investigation 124, 15 p.

Willman, H.B., R.R. Reynolds, and P. Herbert, 1946, Geological aspects of prospecting and areas for prospecting in the zinc-lead district of northwestern Illinois: Illinois State Geological Survey, Report of Investigation 116, 48 p.

APPENDIX: REMOTE SENSING DATA RESOURCES

The remote sensing data resources, including the aerial photographs, vegetated crop line features, LiDAR shaded relief images, sinkholes, and mine digging alignments produced and used for this investigation are included with this publication as four online collections. The collections are available for viewing and download at the following web page: http://isgs.illinois.edu/publications/c589/appendix.Locations of the collections are shown in Figures A1–A4 and Tables A1–A4, and on Map 1.

Crop Line Aerial Photographs—August 2012

The August crop line photographs contain the natural-color, vertical aerial photographs acquired by IDOT on August 28, 2012, as a reconnaissance mission for this study to record vegetated crop lines for 15 selected project areas within Jo Daviess County, Illinois. Figure A1 shows the location of each of the 15 flight lines or strips (ST) of aerial photographs on a regional map of the study area, and Table A1 is a listing of the groups of aerial photographs by strip identification number and township–range.

The film-based aerial photography was acquired using a 9 × 9 in. format Wild aerial camera, and the original film was digitized for each 9 × 9 in. frame by using a high-precision Leica aerial film scanning system at 2,032 dpi to produce full-resolution, archival TIFF images (approximately 1 gigabyte per image). The online collection contains 58 individual frames selected from the original 104 aerial photographs, each of which illustrates vegetated crop lines. To reduce the file size for the online collection, high-quality 300-dpi JPEG images were produced from each archival TIFF. The full-resolution TIFF images are available on request.

Although acquired in a vertical orientation, the digitized aerial photographs have not been georeferenced or orthorectified by using ground control; therefore, the vegetated crop lines visible in each of the aerial photographs were not digitized. Although the images are not georeferenced, each is oriented north-up to facilitate interpretation.

Crop Line Aerial Photographs—September 2012

The September crop line photographs contain the vertical aerial photographs (September 27, 2012, acquisition date) captured from Google Earth (https://www.google.com/earth/) using the Shape2Earth (http://shape2earthengine.com/shape2earth/Home.html) image capture program, which preserves the georeferencing information for the purpose of facilitating GIS and mapping analyses. Figure A2 shows their location on a regional map of the study area, and Table A2 is a listing of the aerial photographs by identification number and township–range.

The vegetated crop lines exhibited on each of the 128 aerial photographs were digitized by using ArcGIS (http://www.arcgis.com/), and the resulting database of 17,855 vegetated crop lines served as the basis for the fracture and crevice analyses.

The Shape2Earth program captured vertical aerial photographs, and the vegetated crop line features were exported directly from the original GIS project database to create layered PDFs. By selecting the Layers navigation panel in Adobe Acrobat Reader or Acrobat Professional (View>Navigation Panels>Layers), the user can toggle on or off the data layer features to view the vegetated crop line features and the original aerial photograph separately. The original ArcGIS file geodatabase containing the georeferenced aerial photographs and digitized crop line features is available on request.

Sinkholes

The sinkhole photographs contain shaded relief images produced from 2008 bare-earth LiDAR for 42 areas within Jo Daviess County that illustrate alignments of sinkhole features. The alignments interpreted directly from the LiDAR data were digitized by using ArcGIS. Figure A3 shows their location on a regional map of the study area, and Table A3 is a listing of the sinkhole areas by identification number and township–range. The LiDAR shaded relief images and digitized sinkhole alignments were exported directly from the original GIS project database to create layered PDFs. By selecting the Layers navigation panel in Adobe Acrobat Reader or Acrobat Professional (View>Navigation Panels>Layers), the user can toggle on or off the data layer features to view the sinkhole alignments and the LiDAR shaded relief image separately. The original ArcGIS file geodatabase containing the LiDAR images and sinkhole alignments is available on request.

Mine Diggings

Photographs of the mine diggings contain shaded relief images produced from 2008 bare-earth LiDAR for 84 areas within Jo Daviess County that illustrate alignments of lead-zinc mine diggings. The alignments interpreted directly from the LiDAR data were digitized by using ArcGIS. Figure A4 shows the mine digging locations on a regional map of the study area, and Table A4 is a listing of the mine digging areas by identification number and township–range. The LiDAR shaded relief images and digitized mine digging alignments were exported directly from the original GIS project database to create layered PDFs. By selecting the Layers navigation panel in Adobe Acrobat Reader or Acrobat Professional (View>Navigation Panels>Layers), the user can toggle on or off the data layer features to view the mine digging alignments and the LiDAR shaded relief image separately. The original ArcGIS file geodatabase containing the LiDAR images and mine digging alignments is available on request.

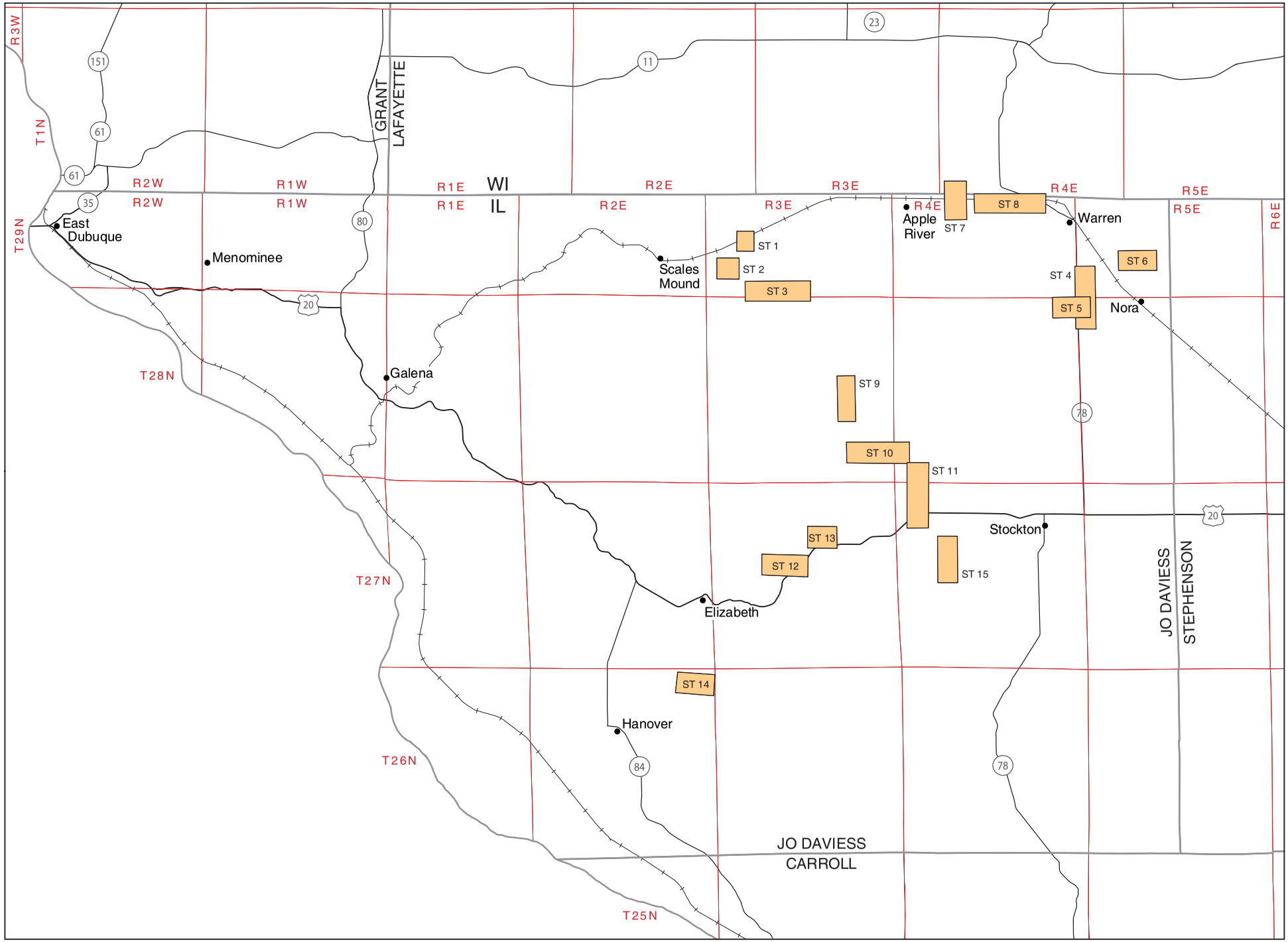

Figure A1 Locations of August 2012 crop line aerial photographs (refer to Table A1). Scale 1 in. = 4 mi (approximate).

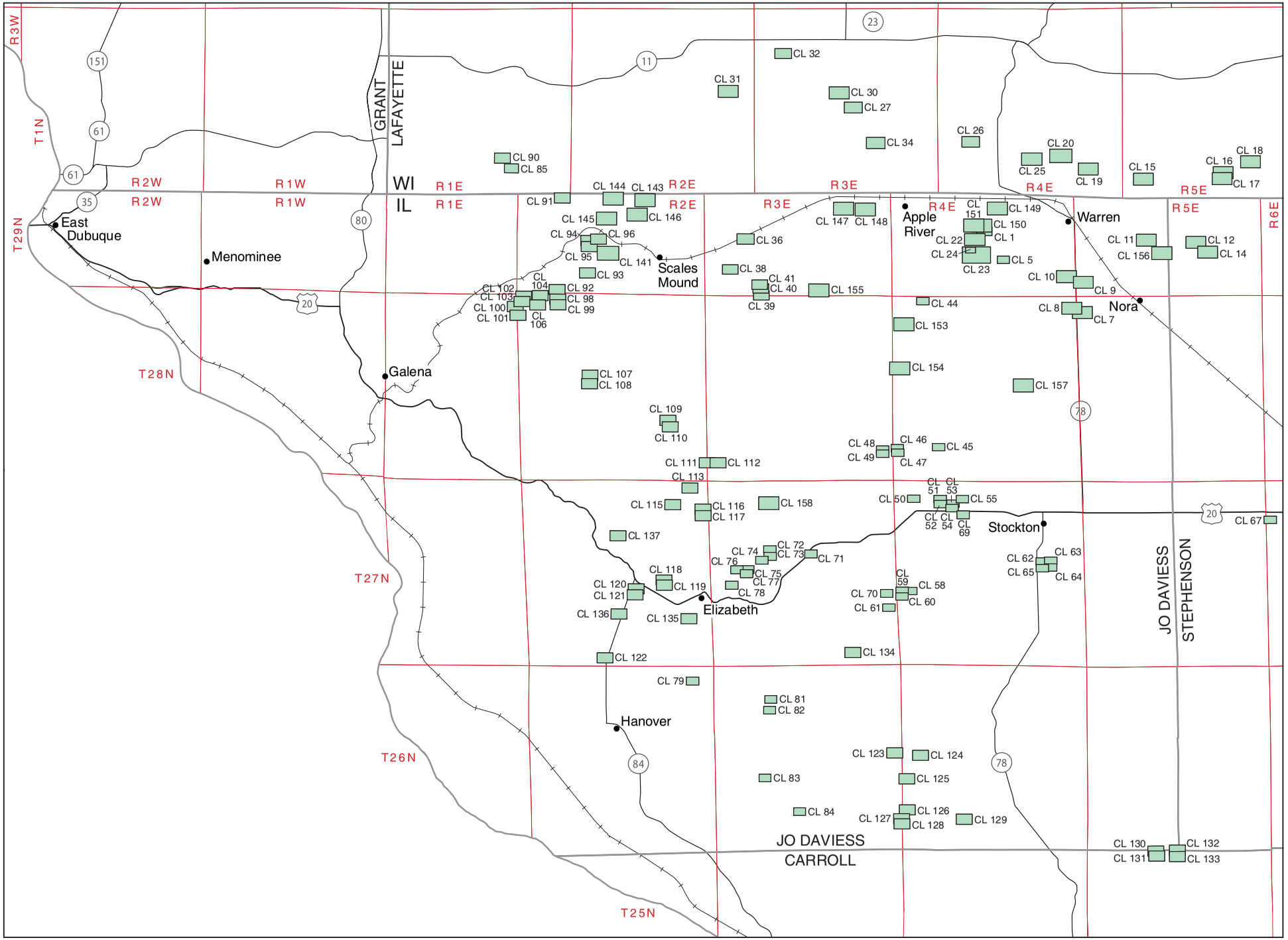

Figure A2 Locations of September 2012 crop line aerial photographs (refer to Table A2). Scale 1 in. = 4 mi (approximate).

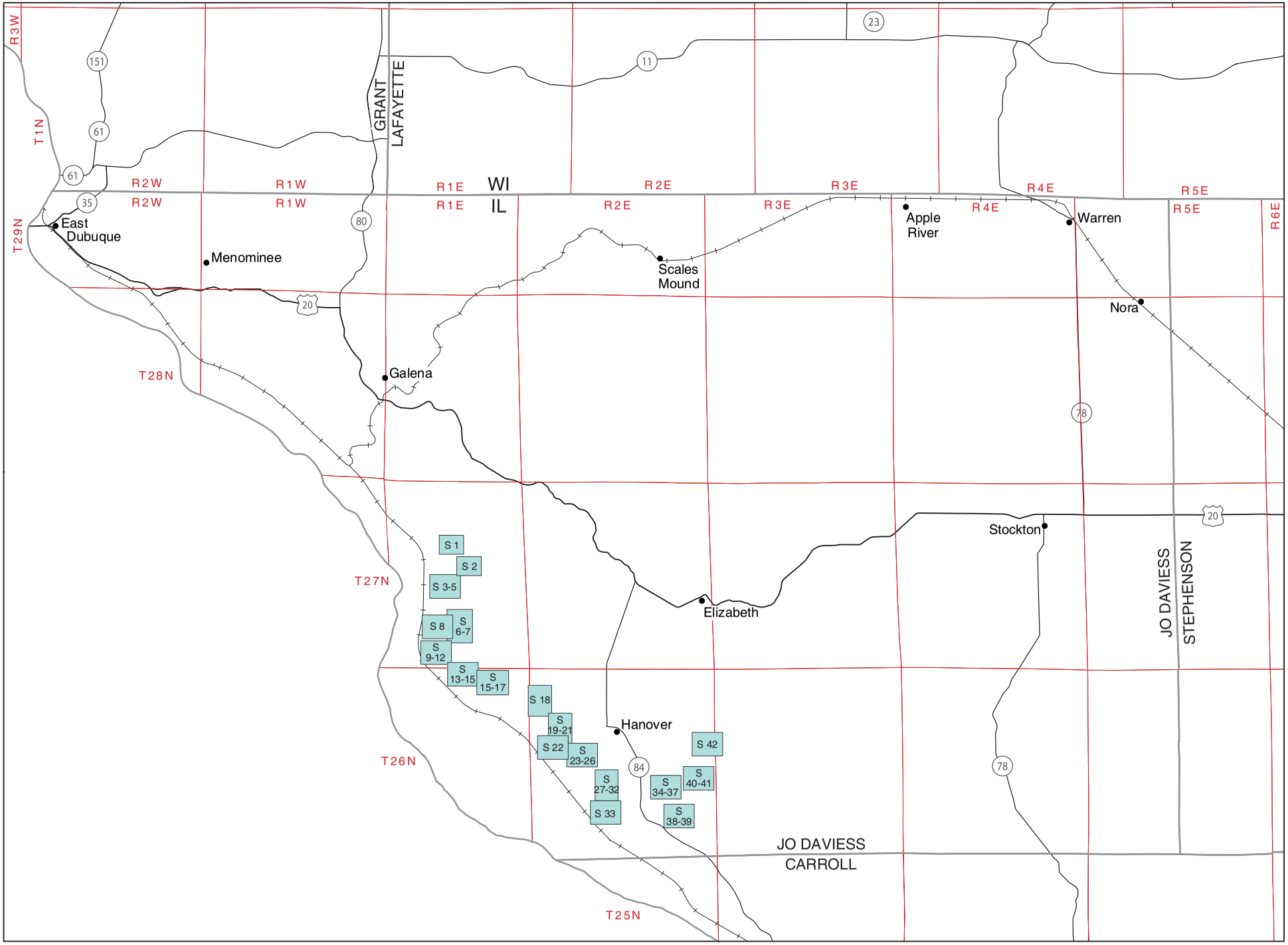

Figure A3 Areas of sinkholes (refer to Table A3). Scale 1 in. = 4 mi (approximate).

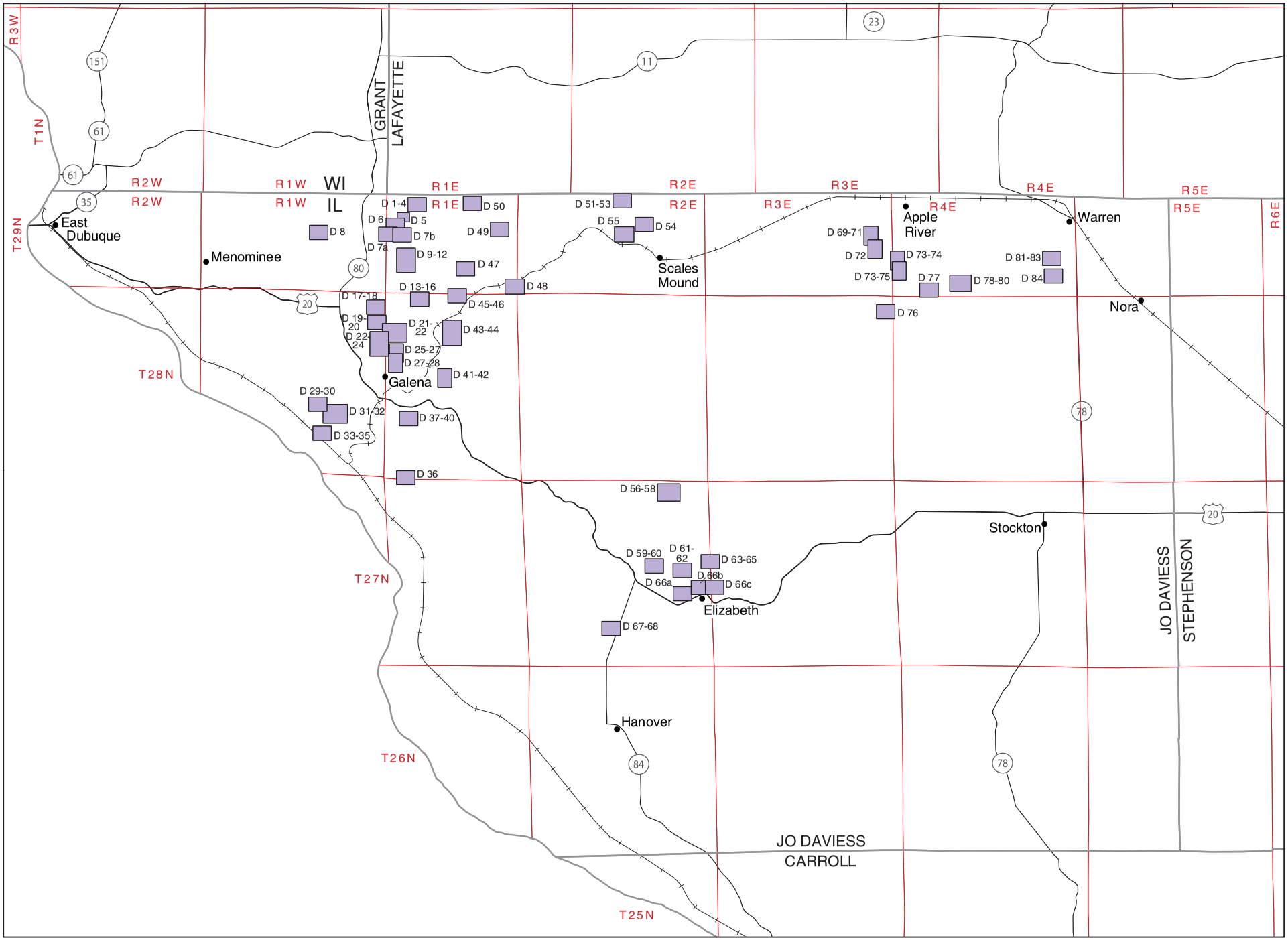

Figure A4 Areas of mine diggings (refer to Table A4). Scale 1 in. = 4 mi (approximate).

Table A1 Listing of August 2012 crop line aerial photographs by township–range location[1]

ID	Township	Range
ST 1	T29N	R3E
ST 2	T29N	R3E
ST 3	T28–29N	R3E
ST 4	T28–29N	R4–5E
ST 5	T28–29N	R4–5E
ST 6	T29N	R5E
ST 7	T29N	R4E
ST 8	T29N	R4E
ST 9	T28N	R3E
ST 10	T28N	R3–4E
ST 11	T27–28N	R4E
ST 12	T27N	R3E
ST 13	T27N	R3E
ST 14	T26N	R2E
ST 15	T27N	R4E

[1]Refer to Figure A1.

Table A2 Listing of September 2012 crop line aerial photographs by township–range location[1]

ID	Township	Range	ID	Township	Range	ID	Township	Range
CL 1	T29N	R4E	CL 61	T27N	R3E	CL 116	T27N	R2–3E
CL 5	T29N	R4E	CL 62	T27N	R4E	CL 117	T27N	R2–3E
CL 7	T28N	R4–5E	CL 63	T27N	R4E	CL 118	T27N	R2E
CL 8	T28N	R4–5E	CL 64	T27N	R4E	CL 119	T27N	R2E
CL 9	T29N	R4–5E	CL 65	T27N	R4E	CL 120	T27N	R2E
CL 10	T29N	R4–5E	CL 67	T27N	R5–6E	CL 121	T27N	R2E
CL 11	T29N	R5E	CL 69	T27N	R4E	CL 122	T27N	R2E
CL 12	T29N	R5E	CL 70	T27N	R3E	CL 123	T26N	R3–4E
CL 14	T29N	R5E	CL 71	T27N	R3E	CL 124	T26N	R4E
CL 15	T1N	R5E	CL 72	T27N	R3E	CL 125	T26N	R3–4E
CL 16	T1N	R5E	CL 73	T27N	R3E	CL 126	T26N	R3–4E
CL 17	T1N	R5E	CL 74	T27N	R3E	CL 127	T26N	R3–4E
CL 18	T1N	R5E	CL 75	T27N	R3E	CL 128	T26N	R3–4E
CL 19	T1N	R4E	CL 76	T27N	R3E	CL 129	T26N	R4E
CL 20	T1N	R4E	CL 77	T27N	R3E	CL 130	T25–26N	R5E
CL 22	T29N	R4E	CL 78	T27N	R3E	CL 131	T25N	R5E
CL 23	T29N	R4E	CL 79	T26N	R2E	CL 132	T25–26N	R5E
CL 24	T29N	R4E	CL 81	T26N	R3E	CL 133	T25N	R5E
CL 25	T1N	R4E	CL 82	T26N	R3E	CL 134	T27N	R3E
CL 26	T1N	R4E	CL 83	T26N	R3E	CL 135	T27N	R2E
CL 27	T1N	R3E	CL 84	T26N	R3E	CL 136	T27N	R2E
CL 30	T1N	R3E	CL 85	T1N	R1E	CL 137	T27N	R2E
CL 31	T1N	R2E	CL 90	T1N	R1E	CL 141	T29N	R2E
CL 32	T1N	R3E	CL 91	T1 & 29N	R1–2E	CL 143	T1 & 29N	R2E
CL 34	T1N	R3E	CL 92	T28–29N	R2E	CL 144	T1 & 29N	R2E
CL 36	T29N	R3E	CL 93	T29N	R2E	CL 145	T29N	R2E
CL 38	T29N	R3E	CL 94	T29N	R2E	CL 146	T29N	R2E
CL 39	T28–29N	R3E	CL 95	T29N	R2E	CL 147	T29N	R3E
CL 40	T29N	R3E	CL 96	T29N	R2E	CL 148	T29N	R3E
CL 41	T29N	R3E	CL 98	T28N	R2E	CL 149	T29N	R4E
CL 44	T28N	R4E	CL 99	T28N	R2E	CL 150	T29N	R4E
CL 45	T28N	R4E	CL 100	T28N	R1–2E	CL 151	T29N	R4E
CL 46	T28N	R3–4E	CL 101	T28N	R1–2E	CL 153	T28N	R4E
CL 47	T28N	R3–4E	CL 102	T28–29N	R1–2E	CL 154	T28N	R3–4E
CL 48	T28N	R3E	CL 103	T28N	R1–2E	CL 155	T28–29N	R3E
CL 49	T28N	R3E	CL 104	T28–29N	R2E	CL 156	T29N	R5E
CL 50	T27N	R4E	CL 106	T28N	R2E	CL 157	T28N	R4E
CL 51	T27N	R4E	CL 107	T28N	R2E	CL 158	T27N	R3E
CL 52	T27N	R4E	CL 108	T28N	R2E			
CL 53	T27N	R4E	CL 109	T28N	R2E			
CL 54	T27N	R4E	CL 110	T28N	R2E			
CL 55	T27N	R4E	CL 111	T28N	R2–3E			
CL 58	T27N	R4E	CL 112	T28N	R3E			
CL 59	T27N	R3–4E	CL 113	T27N	R2E			
CL 60	T27N	R3–4E	CL 115	T27N	R2E			

[1]Refer to Figure A2.

Table A3 Listing of sinkholes by township–range location[1]

ID	Township	Range
S 1	T27N	R1E
S 2	T27N	R1E
S 3–5	T27N	R1E
S 6–7	T27N	R1E
S 8	T27N	R1E
S 9–12	T27N	R1E
S 13–15	T26–27N	R1E
S 15–17	T26N	R1E
S 18	T26N	R1–2E
S 19–21	T26N	R2E
S 22	T26N	R2E
S 23–26	T26N	R2E
S 27–32	T26N	R2E
S 33	T26N	R2E
S 34–37	T26N	R2E
S 38–39	T26N	R2E
S 40–41	T26N	R2E
S 42	T26N	R2–3E

[1]Refer to Figure A3.

Table A4 Listing of mine diggings by township–range location[1]

ID	Township	Range
D 1–4	T29N	R1E
D 5	T29N	R1E
D 6	T29N	R1W–1E
D 7a	T29N	R1W–1E
D 7b	T29N	R1E
D 8	T29N	R1W
D 9–12	T29N	R1E
D 13–16	T28–29N	R1E
D 17–18	T28N	R1W
D 19–20	T28N	R1W–1E
D 21–22	T28N	R1W–1E
D 22–24	T28N	R1 W–1E
D 25–27	T28N	R1E
D 27–28	T28N	R1E
D 29–30	T28N	R1W
D 31–32	T28N	R1W
D 33–35	T28N	R1W
D 36	T27–29N	R1E
D 37–40	T28N	R1E
D 41–42	T28N	R1E
D 43–44	T28N	R1E
D 45–46	T28–29N	R1E
D 47	T29N	R1E
D 48	T28–29N	R1–2E
D 49	T29N	R1E
D 50	T29N	R1E
D 51–53	T29N	R2E
D 54	T29N	R2E
D 55	T29N	R2E
D 56–58	T27N	R2E
D 59–60	T27N	R2E
D 61–62	T27N	R2E
D 63–65	T27N	R2–3E
D 66a–c	T27N	R2–3E
D 67–68	T27N	R2E
D 69–71	T29N	R3E
D 72	T29N	R3E
D 73–74	T29N	R3–4E
D 73–75	T29N	R3–4E
D 76	T28N	R3–4E
D 77	T28–29N	R4E
D 78–80	T29N	R4E
D 81–83	T29N	R4E
D 84	T29N	R4E

[1]Refer to Figure A4.